Inorganic Chemistry

Article

pubs.acs.org/IC

Secondary Coordination Sphere Effects in Ruthenium(III) Tetraammine Complexes: Role of the Coordinated Water Molecule

Maykon L. Souza,[†] Eduardo E. Castellano,[‡] Joshua Telser,[§] and Douglas W. Franco*,[†]

[†]Instituto de Química and [‡]Instituto de Física, Universidade de São Paulo, São Carlos, Brazil

[§]Department of Biological, Chemical and Physical Sciences, Roosevelt University, Chicago, Illinois 60605 United States

Supporting Information

ABSTRACT: The complexes *trans*-$[Ru^{III}(NH_3)_4(4\text{-pic})(H_2O)](CF_3SO_3)_3$ (**1**) and $[Ru^{III}(NH_3)_5(4\text{-pic})](CF_3SO_3)_3$ (**2**) were isolated and studied experimentally by electron paramagnetic resonance (EPR) and UV−vis spectroscopies, cyclic voltammetry, and X-ray crystallography and theoretically by ligand-field theory (LFT) and density functional theory (DFT) calculations. Complex **1** is reported in two different crystal forms, **1a** (100 K) and **1b** (room temperature). EPR and UV−vis spectroscopies suggest that aqua ligand interaction in this low-spin ruthenium(III) complex changes as a function of hydrogen bonding with solvent molecules. This explicit water solvent effect was explained theoretically by DFT calculations, which demonstrated the effect of rotation of the aqua ligand about the N_{pic}−Ru−O_{aq} axis. The UV−vis spectrum of **1** shows in an aqueous acid solution a broad- and low-intensity absorption band around 28 500 cm^{-1} ($\varepsilon \approx 500\ M^{-1}\ cm^{-1}$) that is assigned mainly to a charge-transfer (CT) transition from the equatorial ligands to the Ru β-4d_{xy} orbital (β-LUMO) using DFT calculations. The electronic reflectance spectrum of **1** shows a broad and intense absorption band around 25 500 cm^{-1} that is assigned to a CT transition from 4-picoline to the Ru β-4d_{xz} orbital (β-LUMO) using DFT calculations. The t_{2g}^5 set of orbitals had its energy splitting investigated by LFT. LFT analysis shows that a rhombic component arises from C_{2v} symmetry by a simple π-bonding ligand (H_2O in our case) twisting about the trans (C_2) axis. This twist was manifested in the EPR spectra, which were recorded for **1** as a function of the solvent in comparison with $[Ru(NH_3)_5(4\text{-pic})]^{3+}$ and $[Ru(NH_3)_5(H_2O)]^{3+}$. Only **1** shows an evident change in the **g**-tensor values, wherein an increased rhombic component is correlated with a higher nucleophilicity (donor) solvent feature, as parametrized by the Abraham system.

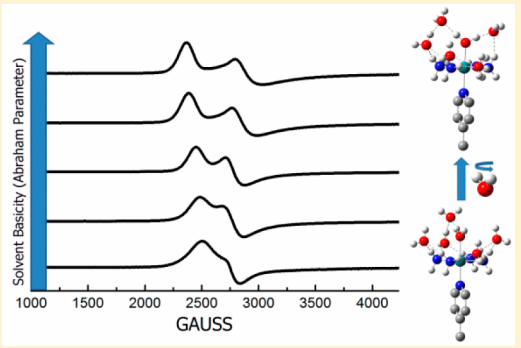

INTRODUCTION

The electronic properties of transition-metal complexes in solution as a function of the chemical and physical properties of the solvent have been studied for decades.[1−7] Stabilization of the Ru^{III} oxidation state in ruthenium(III) tetra- and pentaammine complexes is directly related to the capacity of the nonbonding electrons of solvent molecules to interact with the ammine protons.[1,2] The nature of this interaction is described as weak and characteristic of hydrogen bonding.[1,2] These interactions have an important influence on the electronic transitions [mainly charge-transfer (CT) bands][1,2] and electrochemical properties[3] of ruthenium(III) ammine complexes. However, consideration of these effects on the solid-state structure, electron paramagnetic resonance (EPR) spectroscopy, and reactivity of these complexes has not received much attention.

Inspired by the results of biological and biochemical studies, the effects of the secondary coordination sphere and noncovalent associations such as hydrogen bonds are becoming subjects of increased attention in coordination chemistry.[8−10] Ligands such as ammines and aqua frequently participate in such secondary coordination sphere interactions.[8−11] The nonheme iron enzyme lipoxygenase, for example, had its activity explained as a function of hydrogen-bond formation between amino acids and the aqua/hydroxido ligands (active site containing $Fe^{III}OH$ and $Fe^{II}OH_2$).[12,13] The chemical properties of the generic MOH_2/OH fragment have been explored in various catalytic processes.[14−18] Recently, water oxidation by aquaruthenium(II) polypyridine complexes was described,[14] wherein a series of reactive ruthenium species ($[Ru^{III}OH]^{2+}$, $[Ru^{III}OOH]^{2+}$, $[Ru^{IV}{=}O]^{2+}$, and $[Ru^{IV}OO]^{2+}$) are formed via a mechanism that proposes metal oxidation, disproportionation reactions, and nucleophilic attack by water at neutral pH. Studies with another class of ruthenium compounds also have received attention, namely, the Ru-bda water oxidation catalysts [specifically, $[Ru(bda)(L)_2]$ where, bda = 2,2′-bipyridine-6,6′-dicarboxylate and L = monodentate ligand such as pyridine (py)], wherein the catalytic efficiency was studied as a function of L.[17] Complexes such as $[Ru(bda)(4\text{-pic})_2]$ and $[Ru(bda)(mmi)_2]$ (mmi = 1,3-dimethylimidazolium-2-ylidene) may dramatically change their water oxidation mechanism when one of the pyridyl ligands is replaced by an aqua ligand.

Received: December 24, 2014
Published: February 5, 2015

DOI: 10.1021/ic5030857
Inorg. Chem. 2015, 54, 2067−2080

Our experience with ruthenium nitrosyl complexes of the type *trans*-$[Ru(NO)(NH_3)_4(L)]^{3+}$ suggests that, under biological conditions, $Ru^{II/III}OH_2$ species are the main products after NO release because of reaction with biological reductants (eq 1). The same product is observed by photochemical processes (eq 2).[19]

$$trans\text{-}[Ru^{II}(NO^+)(NH_3)_4(L)]^{3+} + red + H_2O \rightarrow trans\text{-}[Ru^{II}(NH_3)_4(L)(H_2O)]^{3+} + oxi + NO \quad (1)$$

$$trans\text{-}[Ru^{II}(NO^+)(NH_3)_4(L)]^{3+} + H_2O \xrightarrow{h\nu} trans\text{-}[Ru^{III}(NH_3)_4(L)(H_2O)]^{3+} + NO \quad (2)$$

However, information regarding the properties of coordinated water in these complexes and its influence on the ruthenium center and axial ligand (L) is scarce.[20,21] These previous studies were primarily limited to investigation of the kinetics of water substitution.[22−25] With the goal of contributing on this issue, the present work reports the synthesis and crystal structure of the complexes *trans*-$[Ru(NH_3)_4(4\text{-pic})(H_2O)](CF_3SO_3)_3\cdot H_2O$ (**1**; 4-pic = 4-picoline, 4-methylpyridine). The aqua ligand reactivity was investigated by cyclic voltammetry, UV−vis and EPR spectroscopies, and density functional theory (DFT) calculations. The $Ru^{III}OH_2$ bond strength was evaluated through the water substitution rate constant and the calculated pK_a values. DFT and ligand-field theory (LFT) calculations and EPR spectroscopy probed the solvent dependence of the properties of the coordinated water molecule. For comparison, the corresponding complex lacking the aqua ligand, $[Ru(NH_3)_5(4\text{-pic})](CF_3SO_3)_3$ (**2**) was also investigated where appropriate.

EXPERIMENTAL SECTION

General Procedures. All chemicals were reagent-grade (Aldrich, Merck, or JT Baker) and were used without further purification. The solvents were purified as described in the literature.[26] Milli-Q water (18 MΩ) was used throughout the experiments. A Bruker model EMX Plus spectrometer operating at X-band frequency (~9.5 GHz) and coupled to a standard cavity was used to obtain the EPR spectra at liquid-nitrogen temperature (77 K). A Digital Temperature Control System, B-VT-2000, with a dewar insert holder uses liquid nitrogen as a coolant for variable-temperature EPR spectra. Spectra of **1** were recorded as both a powder and a frozen solution at 119, 150, and 175 K. The spectrum at 119 K gave optimal signal/noise although spectra are observable at up to 180 K (see Figure S1 in the Supporting Information, SI), but these higher temperature spectra were not useful for quantitative purposes. UV−vis spectra were recorded using Hitachi U-3501 and Hewlett-Packard diode array model 8452A spectrophotometers. A UV−vis reflectance spectrum of $\mathbf{1}\cdot H_2O$ mixed with $BaSO_4$ was recorded using a diffuse-reflectance accessory from a Shimadzu UV-3600 spectrophotometer. Differential scanning calorimetry (DSC) analysis was performed under a flowing nitrogen atmosphere in the temperature range of +25 to −150 °C at a cooling rate of 10 °C min^{-1} using a TA Instruments DSC-Q20 calorimeter. Voltammetric measurements were carried out with a Princeton Applied Research Polarographic Voltammeter system (model 264) coupled to a microcomputer. The formal reduction potential ($E_{1/2}$) was measured by cyclic voltammetry using a three-electrode cell: (1) saturated calomel (reference electrode); (2) glassy carbon (working electrode); (3) platinum (auxiliary electrode). The $E_{1/2}$ values are listed in relation to a standard hydrogen electrode. The measurements were carried out in $CF_3COOH/NaCF_3COO$ (pH 2.0, μ = 0.2 M) at 25.0 ± 0.2 °C under an argon atmosphere. The acidity of the coordinated water molecule in *trans*-$[Ru(NH_3)_4(4\text{-pic})(H_2O)]^{3+}$ was studied through cyclic voltammetry and UV−vis spectrophotometry. The variations in the $E_{1/2}$ values as a function of the pH were plotted according to a Pourbaix diagram,[27] which allows one to calculate the pK_a value for the following reaction (eq 3):

$$trans\text{-}[Ru(NH_3)_4(4\text{-pic})(OH_2)]^{3+} + H_2O \rightleftharpoons trans\text{-}[Ru(NH_3)_4(4\text{-pic})(OH)]^{2+} + H_3O^+ \quad (3)$$

The pK_a value was also calculated from the spectrophotometric data by a graphical solution of eq 4, where A = absorbance of the mixture, A_p = absorbance of the protonated species, and A_d = absorbance of the deprotonated species.[28]

$$pH = pK_a + \log\frac{A - A_p}{A_d - A} \quad (4)$$

Coordinated water molecule substitution by halide ions (X^- = Cl^-, Br^-) in *trans*-$[Ru(NH_3)_4(4\text{-pic})(H_2O)]^{3+}$ (eq 5) was performed by dissolving the triflate salt in degassed acidic aqueous sodium bromide or chloride solutions (0.5−2 mol L^{-1} in 1.0 × 10^{-2} mol L^{-1} CF_3CO_2H), which were quickly transferred to a quartz cuvette (1 cm path length). The absorbance data were collected at 350 and 420 nm, following in each case the formation of *trans*-$[Ru(NH_3)_4(4\text{-pic})(Cl)]^{2+}$ and *trans*-$[Ru(NH_3)_4(4\text{-pic})(Br)]^{2+}$, respectively.

$$trans\text{-}[Ru(NH_3)_4(4\text{-pic})(OH_2)]^{3+} + X^- \rightleftharpoons trans\text{-}[Ru(NH_3)_4(4\text{-pic})(X)]^{2+} + H_2O \quad (5)$$

Synthesis. The complexes $[RuCl(NH_3)_5]Cl_3$, $[Ru(NH_3)_5(H_2O)](CF_3SO_3)_3$ (**3**), *trans*-$[RuCl(NH_3)_4(SO_2)]Cl$, and *trans*-$[Ru(SO_4)(NH_3)_4(4\text{-pic})]Cl$ were prepared from $RuCl_3\cdot 3H_2O$ as described in the literature.[29−31]

$[Ru(NH_3)_5(4\text{-pic})](CF_3SO_3)_3$ (2). $[Ru(NH_3)_5(4\text{-pic})](ClO_4)_2$ and the aqueous Ru^{III} ion, $[Ru(NH_3)_5(4\text{-pic})]^{3+}$, were prepared as described in the literature.[32] A CF_3SO_3H solution (6.0 mol L^{-1}) was used to precipitate the complex as the triflate salt. To obtain crystals, the dry solid (100 mg) was completely dissolved in 5 mL of CF_3SO_3H (0.2 mol L^{-1}) and filtered and the solution maintained at 5 °C for 2 days. The yellow crystals formed were separated by filtration (0.07 mmol, yield 52%).

***trans*-$[Ru(NH_3)_4(4\text{-pic})(H_2O)](CF_3SO_3)_3$ (1).** A total of 100 mg of *trans*-$[Ru(SO_4)(NH_3)_4(4\text{-pic})]Cl$ (0.25 mmol) was added to 1.0 mL of a degassed CF_3CO_2H solution (1.0 × 10^{-3} mol L^{-1}) containing pieces of Zn (Hg). The reaction mixture remained under a constant flow of argon for 20 min. The resulting red solution was transferred to a previously degassed flask, and 39 μL of 30% H_2O_2 (0.38 mmol) was added. The resulting pale-yellow solution was immediately transferred for another flask containing 2.5 mL of a degassed solution of CF_3SO_3H (6 mol L^{-1}). An air-stable and fine yellow crystalline precipitate was immediately formed. The mixture was maintained at 5 °C for 3 h to ensure complete precipitation. The solid obtained was separated by filtration and exhaustively dried under vacuum. To obtain crystals, the dry solid (130 mg) was completely dissolved in 6 mL of CF_3SO_3H (2 mol L^{-1}) and filtered and the solution maintained at 5 °C for 2 days. The yellow crystals formed were separated by filtration (0.11 mmol, yield 43%).

X-ray Data Collection and Structure Determination. A summary of the crystal data and detailed refinement conditions for **1**, solved at 100 K (**1a**) and room temperature (**1b**), and **2**, solved at room temperature, are given in the SI (X-ray data collection and Table S1). Listings of atomic coordinates and equivalent isotropic displacement parameters, full intramolecular bond distances and angles, hydrogen coordinates, and anisotropic thermal parameters are available from the authors and were deposited at the Cambridge Crystallographic Data Centre (CCDC), reference numbers CCDC 999499 (**1a**), 886779 (**1b**), and 980664 (**2**).

DOI: 10.1021/ic5030857
Inorg. Chem. 2015, 54, 2067−2080

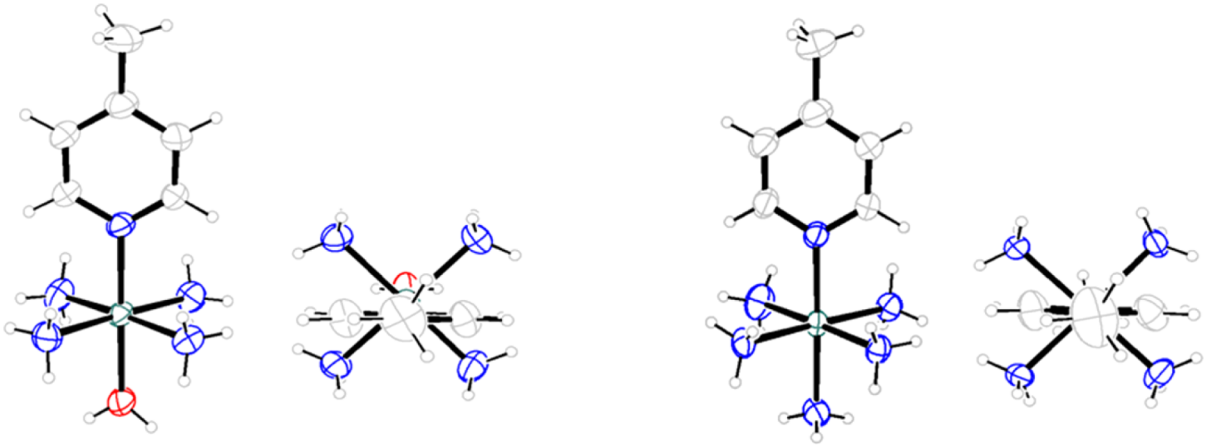

Figure 1. ORTEP plots of two different views of *trans*-$[Ru(NH_3)_4(4\text{-pic})(H_2O)]^{3+}$ (cation of **1**; left) and $[Ru(NH_3)_5(4\text{-pic})]^{3+}$ (cation of **2**; right) both with displacement ellipsoids shown at the 30% probability level. The $CF_3SO_3^-$ anions were omitted for clarity.

Table 1. Interatomic Distances (Å) and Angles (deg) for *trans*-$[Ru(NH_3)_4(4\text{-pic})(L)]^{n+}$ [L = H_2O (1), NH_3 (2), Cl^-, and SO_4^{2-}]

	distance (Å)			angle (deg)	
L	Ru−L	Ru−N_{pic}	Ru−NH_3	L−Ru−N_{pic}	NH_3−Ru−NH_3
H_2O[a]	2.043(5)	2.050(5)	2.111(9)	178.5(2)	176.9(2)
H_2O[b,c]	2.025(4)	2.050(5)	2.109(8)	177.3(18)	176.4(19)
H_2O[b,d]	2.049(4)	2.037(5)	2.114(6)	177.6(18)	176.9(19)
Cl^- [e]	2.344(9)	2.074(2)	2.105(6)	179.0(8)	179.64(8)
SO_4^{2-} [f]	2.046(2)	2.064(2)	2.104(4)	175.2(1)	179.21(7)
NH_3[a]	2.118(5)	2.083(5)	2.108(6)	178.97(16)	178.54(17)

[a]This work (solved at room temperature). [b]This work (solved at 100 K). [c]Independent complex $\mathbf{1a_1}$. [d]Independent complex $\mathbf{1a_2}$. [e]Reference 46. [f]Reference 47.

THEORETICAL APPROACH AND COMPUTATIONAL DETAILS

DFT Quantum Calculations. Spin-unrestricted DFT calculations were performed with the *Gaussian03* package.[33] The optimizations were performed using Kohn−Sham DFT with the hybrid B3LYP exchange-correlation functional and the basis set DGDZVP for ruthenium and LANL2DZ for the ligands. The BP86 functional and other basis sets also were initially tested (see Table S2 in the SI). However, the B3LYP/DGDZVP-LANL2DZ basis set provides the best relationship between the results and computational cost. No symmetry condition was imposed. Implicit solvent effects were included using the integral equation formalism polarized continuum model (IEF-PCM) with water as the solvent. Vibrational frequency calculations were performed at the same level of theory for all optimized structures to verify that no imaginary frequencies were present and to ensure the true local minima energy. The modeling of an explicit solvent effect (Figure S2 in the SI) was performed with a discrete number of water molecules (see geometry optimization in the SI for more details). Single-point energy calculations were performed on optimized structures using the B3LYP functional with DGDZVP (ruthenium) and a larger basis set than LANL2DZ for all other atoms, the DGTZVP. Time-dependent DFT (TD-DFT) calculations were done at the same level of theory. The energies and intensities of the 80 lowest singlet-energy electronic transitions of the complexes were performed in the TD-DFT calculations. Orbital contour plots were generated using *Gaussview 04*; analysis of the population and TD-DFT data was done with *GaussSum 3.0*.[34]

LFT Calculations. Several LFT programs were employed. The first program, DLSD5, is based on work by McGarvey et al.[20,35] It is available from J. Telser and was used previously in a study of low-spin (LS) Fe^{III} complexes,[36] which described in detail its operation. DLSD5 uses as input the three observed g values and outputs the calculated best-fit ligand-field parameters: k, Δ/ζ, and V/ζ, which correspond to the orbital reduction factor ($k \leq 1$), and the axial and rhombic ligand-field splittings within the $^2T_{2g}$ ground state ($t_2^5e^0$ in a strong field representation) of octahedral LS d^5. These are defined so that $|d_{xy}^{\pm}\rangle$ is at energy Δ and $|d_{xz}^{\pm}\rangle$ and $|d_{yz}^{\pm}\rangle$ are at energies $+V/2$ and $-V/2$, respectively (disregarding spin−orbit coupling, SOC). These ligand-field parameters are normalized by the one-electron SOC constant, ζ, which is not well-determined for free-ion Ru^{III},[37] but values of 800−1000 cm^{-1} are commonly used;[20,35] e.g., a value ζ = 880 cm^{-1} was estimated for Ru^{III} in $(Ph_4As)_3[Ru(CN)_6]\cdot 2H_2O$.[38] We will use here ζ = 800 cm^{-1}, simply to be on the conservative side in terms of SOC effects. We are concerned here only with relative comparisons among closely related systems and not with the actual values of the ligand-field parameters. The second program used, DDN, performs LFT calculations employing the full d^5 basis set (252 microstates), is also available from J. Telser, and has been used in studies of other transition-metal ion systems, such as LS Mn^{III}.[39] The very powerful LFT program *Ligfield*, by Bendix et al., was also used.[37] *Ligfield* provides a description of the d orbital occupancy of the ground-state doublet using these models and confirms the energy levels calculated by DDN.

DOI: 10.1021/ic5030857
Inorg. Chem. 2015, 54, 2067−2080

RESULTS AND DISCUSSION

Molecular Structures. Crystallographic data for the isolated complexes **1** and **2** are given in Table S1 in the SI and as ORTEP representations in Figure 1. Table 1 summarizes the bond lengths and angles for **1**, **2**, and other selected ruthenium(III) complexes. The Ru^{III} ion in both **1** and **2** is very close to being in a regular octahedral environment with the aromatic moiety perpendicular to the plane through the four ammine equatorial nitrogen atoms and bisecting two opposite N−Ru−N angles.

At 100 K, the crystal of **1** has a unit cell composed of two crystallographically independent complexes (**1a**$_1$ and **1a**$_2$; see the X-ray data collection in the SI) and three noncoordinated water molecules (W1, W2, and W3; Figure S3 in the SI). The two complexes have slightly different bond distances in the N_{pic}−Ru−O_{aq} axis (see Table 1). The X-ray data show that the three noncoordinated water molecules are distributed such that two of them are closer to **1a**$_1$ (distances of 2.50 and 4.10 Å from the aqua ligand respectively for W1 and W2), while the third noncoordinated water molecule (W3) is 2.71 Å from the aqua ligand in **1a**$_2$. W2 is only 2.70 Å from W1, which suggests a strong hydrogen-bonding interaction between the two. This interaction may explain the shorter distance between W1 and the aqua ligand in **1a**$_1$ in comparison to that observed for W3 and **1a**$_2$. In each independent complex, there is a close by $CF_3SO_3^-$ anion, with one of its oxygen atoms located 2.62 Å (**1a**$_1$) and 2.69 Å (**1a**$_2$) from the aqua ligand oxygen atom. All of these observed distances are compatible with strong hydrogen bonding. The shorter anion distance in **1a**$_1$ is consistent with the shorter Ru−O_{aq} bond length in **1a**$_1$ relative to **1a**$_2$ (see Table 1 and Figure S3 in the SI).

At room temperature, the crystal quality of **1** decreases and only one crystallographically independent complex and one noncoordinated water molecule, which is 2.58 Å from the coordinated water, can be seen. Because the crystals solved at 100 K and room temperature are the same, the absence of the half water molecule in **1** can be ascribed to crystal disorder. Indeed, the crystal structures described in this work are characterized by some disorder in the $CF_3SO_3^-$ anion, which appears to be caused by the highly charged character of the cations and the consequent strong hydrogen bonding originating from the counteranions' interactions with water molecules, mainly regarding the coordinated water. These features result in structures that do not present high diffraction quality, as pointed out and explained in the CIF archives (SI). Despite this, some interesting properties were observed, such as that the unit cell volume of **1** changes from 5339.6(5) Å^3 at 100 K to 2784.64(18) Å^3 at room temperature. This transition happens in a totally reversible way without crystal destruction. A DSC experiment suggested an endothermic process at 180 K (Figure S4 in the SI) that may correspond to this transition. In contrast, DSC gives no evidence for any phase transition in **2**, which is an "aqua-free" analogue to **1**. Although apparently there are no reports about this phenomenon specifically in ruthenium ammine complex crystals, this is a relatively common process in crystalline organic structures and metallic complexes unleashed by changes in pressure,[40] temperature,[41,42] solvent crystallization,[43,44] and hydrogen-bonding interaction.[45] In particular, the phase transitions reported[45] for the coordination polymers $[Cu(NCS)_2(L)]_n$ (L = 4-aminopyridine and 4-methylaminopyridine) were quite affected by the motion of the NCS^- group and by hydrogen bonding. In this case, a considerable displacement of the NCS^- group was reported and associated with the phase transition. The phase transition in complex **1** needs to be more deeply investigated in future work, which could evaluate the influence not only of the solvent but of the counterion as well. Currently, we are unable to obtain crystals with counterions other than triflate, and even those crystals do not exhibit high diffraction quality, albeit sufficient for our purposes. This difficulty may be the result of the high displacement factors generated not only in the three triflate ions but also in the aqua ligand and crystallization water molecules owing to strong hydrogen bonding as reported for $[Cu(NCS)_2(L)]_n$.

Water Ligand Properties: pK_a and Lability. The reactivity of the aqua ligand was briefly studied in terms of its acidity and replacement by chloride and bromide ions. The electronic spectrum of *trans*-$[Ru(NH_3)_4(4\text{-pic})(H_2O)]^{3+}$ as a function of the pH is presented in Figure 2. The intense

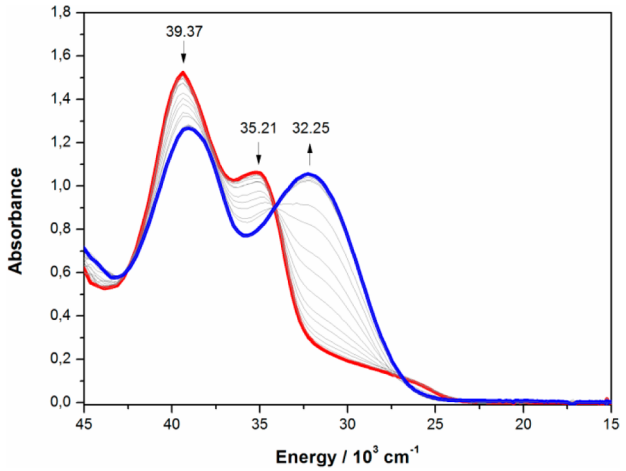

Figure 2. Electronic spectrum as a function of the pH for a solution containing *trans*-$[Ru^{III}(NH_3)_4(4\text{-pic})(H_2O)]^{3+}$ ion. $C_{Ru} = 2.8 \times 10^{-4}$ M; μ = 0.1 M (CF_3CO_2Na); extreme pH values are shown as 2 (red line) and 7.7 (blue line).

absorption around 32 250 cm^{-1} at pH > 6 can be associated with the formation of *trans*-$[Ru(NH_3)_4(4\text{-pic})(OH)]^{2+}$ (eq 3). This absorption is associated with coordination by a better π donor than water, namely, hydroxide ion, and may be assigned to a pπ(OH) → 4dπ ligand-to-metal charge-transfer (LMCT) band. This assignment is analogous to that made for other ions in the series *trans*-$[Ru^{III}(NH_3)_4(4\text{-pic})(L)]^{n+}$, where L is chloride, bromide, iodide, and sulfate.[47] According to the observed LMCT energies for this series, the water ligand is a poorer π donor than hydroxide ion, as expected from the spectrochemical series $NH_3 < H_2O < OH^- < SO_4^{2-} < Cl^- < Br^- < I^-$. TD-DFT calculations have provided theoretical support for this assignment (see the Electronic Structure section).

In the electrochemical study, the formal reduction potential ($E_{1/2}$) for the Ru^{III}/Ru^{II} couple is shifted to more negative values as the pH is increased (Figure S5 in the SI). That shift is in agreement with Ru^{III} being more stabilized in *trans*-$[Ru^{III}(NH_3)_4(4\text{-pic})(OH)]^{2+}$ than in *trans*-$[Ru^{III}(NH_3)_4(4\text{-pic})(H_2O)]^{3+}$. Both electronic spectra and cyclic voltammetry measurements (see Figures S6 and S7 in the SI), in concordance, gave pK_a = 3.65 ± 0.05. This is an intermediate value in comparison to those reported[21] for

DOI: 10.1021/ic5030857
Inorg. Chem. 2015, 54, 2067−2080

Table 2. Summary of Selected Interatomic Distances (Å), pK_a Values, and Water Substitution Rate Constants (k_{-H_2O}, M^{-1} s^{-1}) for Ruthenium Aqua Species

complex	d(Ru−OH_2)	pK_a	$k_{-H_2O}(Cl^-)$ at 40 °C	$k_{-H_2O}(Cl^-)$ at 55 °C	$k_{-H_2O}(Br^-)$ at 55 °C
$[Ru^{III}(NH_3)_5(H_2O)]_2[S_2O_6]_3$	2.110[a]	4.1[b]	8.7×10^{-5} [b]	2.1×10^{-3} [c]	1.3×10^{-3} [c]
trans-$[Ru^{II}(NO)(NH_3)_4(H_2O)]Cl_3$	2.040[b]	3.1[b]	3.7×10^{-6} [b]		
trans-$[Ru^{III}(NH_3)_4(4\text{-pic})(H_2O)](CF_3SO_3)_3$	2.043[d]	3.6[d]	3.4×10^{-5}[d]	2.5×10^{-4} [d]	1.5×10^{-4} [d]

[a]Reference 48. [b]Reference 21. [c]Reference 25. [d]This work (solved at room temperature).

$[Ru^{III}(NH_3)_5(H_2O)]^{3+}$ and *trans*-$[Ru^{II}(NH_3)_4(NO)(H_2O)]^{3+}$ and suggests a stronger Ru−OH_2 bond in the 4-picoline species than in the pentaammines. A similar trend was provided by the rate constant for water replacement (k_{-H_2O}); see Table 2.

When the trans NH_3 ligand in $[Ru(NH_3)_5(H_2O)]^{3+}$ is changed to L = 4-picoline or nitric oxide, *trans*-$[Ru(NH_3)_4(L)(H_2O)]^{3+}$, then the rate constant for substitution of the aqua ligand by Cl^- (to give *trans*-$[Ru(NH_3)_4(L)(Cl)]^{n+}$) decreases respectively by approximately 2.5- and 23-fold at 40 °C. Because 4-picoline, unlike NH_3, is a π-acceptor ligand, the stronger Ru−OH_2 bond in *trans*-$[Ru^{III}(NH_3)_4(4\text{-pic})(H_2O)]^{3+}$ versus $[Ru^{III}(NH_3)_5(H_2O)]^{3+}$ can be ascribed to an increase in the ruthenium π acidity. The same effect results from the replacement of NH_3 by the strong π-acceptor NO^+, as reported for *trans*-$[Ru^{II}(NH_3)_4(NO)(H_2O)]^{3+}$.[21] Also this is likely the reason for the lower pK_a of *trans*-$[Ru^{III}(NH_3)_4(4\text{-pic})(H_2O)]^{3+}$ and *trans*-$[Ru^{II}(NH_3)_4(NO)(H_2O)]^{3+}$ relative to $[Ru^{III}(NH_3)_5(H_2O)]^{3+}$.

To gain more insight about the electronic effect of the 4-picoline ligand and hydrogen bonding of the H_2O ligand, DFT and LFT theoretical approaches and EPR spectroscopy were applied to both *trans*-$[Ru^{III}(NH_3)_4(4\text{-pic})(H_2O)]^{3+}$ and $[Ru^{III}(NH_3)_5(4\text{-pic})]^{3+}$ complexes. The parameters and molecular reference frame considered in these studies are illustrated in Chart 1. The choice of the ligand-field coordinate system for these complexes, as shown in Chart 1 (upper), is based on their own crystal structures (Figure 1) and on previous work on related systems: $[Ru(NH_3)_5X]^{2+}$, where X^- = Cl^- and Br^-.[49] These pentaammine complexes are, to our knowledge, the only relevant complexes for which the **g** matrix orientation has been definitively determined, by single-crystal EPR, and exhibit $g_z = g_{max}$ along the "*trans*" X−Ru−NH_3 axis (Chart 1, upper right). What is different in our tetraammine complexes relative to these $[Ru(NH_3)_5X]^{2+}$ complexes is the relative orientation of the π-interacting ligands, *trans* 4-picoline and aqua, which are parametrized respectively by ψ_L and ψ_{OH_2} (Chart 1, upper left).

Chart 1. Molecular Reference Frame Applied to the Ruthenium(III) complexes of Interest, Primarily *trans*-$[Ru^{III}(NH_3)_4(4\text{-pic})(H_2O)]^{3+}$ but Also $[Ru^{III}(NH_3)_5X]^{2+}$ (X = Halide and Other Ligands)[a]

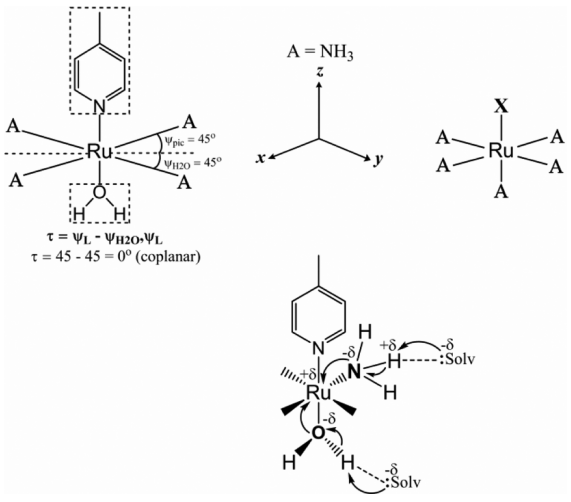

[a]The twist effect of the H_2O ligand plane related to the 4-picoline plane (upper and left sides, as given initially by $\psi_{OH_2} = \psi_L = 45°$) on the *g* values was investigated by LFT. Chart 1 (lower) shows the solvent interactions that were probed by DFT calculations.

Optimized Structures (DFT). The *trans*-$[Ru^{III}(NH_3)_4(4\text{-pic})(H_2O)]^{3+}$ and $[Ru^{III}(NH_3)_5(4\text{-pic})]^{3+}$ complexes were optimized considering up to five free water molecules ideally distributed in the vicinity of the ligands (Figure S2 in the SI). The optimized geometries present bond distances in good agreement with the X-ray data; see Table 3. The calculated Ru−L bond lengths are up to 0.058 Å (~3%) longer than the experimental values, which is expected with the B3LYP functional.[50,51] The complex *trans*-$[Ru(NH_3)_4(4\text{-pic})(H_2O)]^{3+}$ (**opt-0**), which is absent of any free water molecule(s), exhibits the longest Ru−O_{aq} bond length among the optimized geometries. The inclusion of a free water molecule produces a structure containing a hydrogen-bonded aqua ligand. This optimized structure, *trans*-$[Ru(NH_3)_4(4\text{-pic})(H_2O)]^{3+}\cdot H_2O$ (**opt-1**), presents bond distances even more consistent with the X-ray data than **opt-0**. This result points to the Ru−O_{aq} bond distance being strongly dependent on the hydrogen-bonding interaction of the hydrogen atoms, as the crystallographic data have indicated. The calculated energy involved in the formation of **opt-1** from *trans*-$[Ru(NH_3)_4(4\text{-pic})(H_2O)]^{3+}$ and H_2O showed a stabilization at about −79.5 kJ mol^{-1}. This value is consistent with those reported for hydrogen bonds involving water molecules as donors.[52]

Zerner and Pearl[1] studied the effect of an explicit water solvent in $[Ru(NH_3)_5(py)]^{3+}$ with ab initio (Hartree−Fock level of theory) and semiempirical quantum-chemical (quantum mechanics/molecular mechanics, QM/MM) techniques. The QM/MM calculations with dozens of water molecules produced structures with an average intermolecular bond distance of 2.75 Å for N(NH_3)−O(H_2O solvent). In these calculations, a comparison with ideal systems containing only 4−6 explicit nearest-neighbor water molecules showed a reduced CT from the solvent to the complex. This effect was ascribed to the extra CT provided by the solvent−solvent interaction, which likely disperses the positive charge of the cation complex over a greater number of solvent molecules. Nevertheless, Zerner and Pearl showed that the idealized systems with nearest-neighbor water molecules, carried out at the Hartree−Fock level of theory, can provide structural and spectroscopic results that are accurate enough to be used in conjunction with QM/MM calculations. In our data, a comparison between $[Ru(NH_3)_5(4\text{-pic})]^{3+}$ and *trans*-[Ru-

DOI: 10.1021/ic5030857
Inorg. Chem. 2015, 54, 2067−2080

Table 3. Experimental and DFT-Calculated Geometry Distances, in Å, for *trans*-$[Ru(NH_3)_4(4\text{-pic})(H_2O)]^{3+}$

	experimental			calculated			
bond	**1a$_1$**[a]	**1a$_2$**[a]	**1b**[b]	**opt-0**	**opt-1**	**opt-5a**	**opt-5b**
Ru−OH_2	2.025	2.049	2.045	2.103	2.061	2.089	2.063
Ru−N(4-pic)	2.055	2.037	2.055	2.073	2.093	2.094	2.109
Ru−$N(NH_3)$	2.109	2.114	2.110	2.165	2.165	2.159	2.160
H_2O[c]···OH_2[d]	2.500	2.713	2.580		2.458	2.594	2.551
HOH[c]···OH_2[d]					1.398	1.576	1.538
H−O				0.977	0.976	0.975	1.004
O−H				0.977	1.058	1.018	1.018

[a]Values taken from the crystal solved at 100 K. **1a$_1$** and **1a$_2$** are the crystallographically independent complexes (see the description on the previous section). [b]Values taken from the crystal solved at room temperature. [c]Coordinated water molecule. [d]Water solvent molecule.

Table 4. Energy and Composition of the Main MOs Calculated (DFT) for the *trans*-$[Ru(NH_3)_4(4\text{-pic})(L)]^{n+}$ Geometries

				% contribution			
geometry (L)	MO	assignment	*E* (eV)	Ru	4-pic	L	NH_3
NH_3	LUMO+1	$\pi_{pic(1v)}^* - d_{xz}$	−2.09	2	97	0	0
	LUMO	$d_{xy,z^2,xz}$	−4.71	95	0	0	4
	HOMO	$d_{xz} - \pi_{pic(3o)}^*$	−7.41	80	16	0	3
	HOMO−1	d_{yz}	−7.66	94	0	1	5
Opt-5a	LUMO+1	$\pi_{pic(1v)}^* - d_{xz}$	−2.13	2	97	0	0
	LUMO	d_{xy}	−4.87	96	0	0	4
	HOMO	$d_{xz} - \pi_{pic(3o)}^* - \mathbf{1b_2}(aq)$	−7.26	72	18	1	8
	HOMO−1	d_{yz}	−7.84	93	0	1	5
Opt-5b	LUMO+1	$\pi_{pic(1v)}^* - d_{xz}$	−2.16	5	94	0	0
	LUMO	$d_{xz,yz} - \pi_{pic(3o)}^* - \mathbf{1b_2}, \mathbf{1b_1}(aq)$	−4.67	84	8	5	2
	HOMO	d_{xy}	−7.47	93	0	0	6
	HOMO−1	$d_{yz,xz} + \pi_{pic(3o)}^* - \mathbf{1b_2}, \mathbf{1b_1}(aq)$	−7.53	86	8	3	2
OH	LUMO+1	$\pi_{pic(1v)}^* - d_{xz}$	−1.91	7	92	1	0
	LUMO	$d_{xz} - p_z(OH) - \pi_{pic(3o)}^*$	−4.00	70	10	18	2
	HOMO	$d_{yz} - p_y(OH)$	−6.94	86	1	10	4
	HOMO−1	d_{xy}	−7.24	94	0	0	6

$(NH_3)_4(4\text{-pic})(H_2O)]^{3+}$ showed that the addition of five explicit water molecules to each geometry produced similar solvent−ammine ligand interactions in the equatorial plane but a stronger interaction with the axial aqua ligand of *trans*-$[Ru(NH_3)_4(4\text{-pic})(H_2O)]^{3+}$. Both geometries have distances of $N(NH_3)$−$O(H_2O$ solvent) in the range of 2.8−2.9 Å, while the aqua complex has distances of $O(H_2O$ ligand)−$O(H_2O$ solvent) in the range of 2.55−2.62 Å.

Certainly, in the absence of a large number of water solvent molecules, the explicit solvent effect is relatively underestimated. However, for our purposes, namely, the influence of this effect on the axial bonds (mainly on the Ru−O_{aq} bond), the number of solvent molecules is sufficient. Indeed, the optimized geometry **opt-5b** illustrates the effect on the axial bond lengths when two of five water molecules interact with the aqua ligand. The calculated interactions in **opt-5b** demonstrate an elongation of the both O−H bonds in the aqua ligand and its rotation in relation to the 4-picoline plane compared to **opt-5a** (aligned aqua ligand). Both effects seem to contribute to the decrease of the Ru−OH_2 bond length in **opt-5b** in relation to **opt-5a** and can represent theoretically the transformation observed in the crystal of **1** when it is cooled from room temperature, during which the N_{pic}−Ru−O_{aq} axial distances slightly decrease.

Electronic Structure. The frontier molecular orbitals (MOs) calculated for **opt-5a**, **opt-5b**, $[Ru(NH_3)_5(4\text{-pic})]^{3+}\cdot 5H_2O$, and *trans*-$[Ru(NH_3)_4(4\text{-pic})(OH)]^{2+}$ are tabulated in Table 4 and depicted in Table S6 in the SI. Owing to the similar features of the σ bonding of a e_g set of orbitals in both α- and β-spin functions and considering that the only unoccupied t_{2g} function (hole) is a β-spin function, as expected for a LS Ru^{III} complex (t_{2g}^5), we limit ourselves to analyzing only the β-spin set of orbitals. The LUMO+1 (LUMO = lowest unoccupied MO) in all complexes is a π^* orbital of the 4-picoline ligand that lies between the t_{2g} and e_g sets of orbitals and is labeled as $\pi_{pic(1v)}^*$ (see Chart S1 in the SI). Although LUMO+1 is essentially centered in the 4-picoline ligand, this orbital has a small contribution from ruthenium (d_{xz}), which seems to be a function of the π-donor ability of the L ligand in *trans*-$[Ru(NH_3)_4(4\text{-pic})(L)]^{n+}$: increasing from 2% (**opt-5a** and pentaammine) to 5% (**opt-5b**) and to 7% (hydroxo complex). The LUMO, highest occupied MO (HOMO), and HOMO−1 are formed by the t_{2g} set of orbitals with a significant contribution of an occupied 4-picoline orbital ($\pi_{pic(3o)}^*$), while the LUMO+2, LUMO+3, and LUMO+4 are formed by

DOI: 10.1021/ic5030857
Inorg. Chem. 2015, 54, 2067−2080

the e_g set of orbitals and another π^* orbital of the 4-picoline ligand, labeled $\pi_{pic(2v)}^*$ (see Chart S1 in the SI). It is possible to observe (Table 4) that the LUMO, HOMO, and HOMO−1 in **opt-5a** and **opt-5b** also present a slight contribution of orbitals originating from the aqua ligand with $\mathbf{1b_1}$ (antibonding) and $\mathbf{1b_2}$ (nonbonding) symmetry (see Chart S2 in the SI). The d_{xz} and d_{yz} orbitals in **opt-5b** are mixed, which is a function of the aqua ligand twist that also promotes the interaction of ruthenium with water for $\mathbf{1b_1}$.

The experimental absorption spectra of **1** and **2** in an aqueous acid solution are formed by broad and weak bands in the visible range but with a high-intensity absorption in the UV region, which can be ascribed to a $\pi \rightarrow \pi^*$ transition in the 4-picoline ligand, as described for similar systems.[7] The absorption spectra of **1** and **2** (Table 5 and Figures 3 and 4)

Table 5. Main Experimental and TD-DFT-Calculated Bands and Their Assignments

exptl, 10^3 cm^{-1} (ε, M^{-1} cm^{-1})	calcd (f)	assignment
	trans-$[Ru(NH_3)_4(4\text{-pic})(H_2O)]^{3+}$ *	
28.50 (~500)	27.89 (0.0018)	very mixed; $NH_3 \rightarrow$ 4d Ru
	27.99 (0.0023)	H−5(β) → L+0(β); $NH_3 \rightarrow$ 4d Ru
		H−10(β) → L+0(β); $NH_3 \rightarrow$ 4d Ru
	28.74 (0.0015)	H−0(β) → L+1(β); 4d Ru, pic → pic
35.21 (4300)	35.27 (0.0123)	H−1(α) → L+3(α), pic → pic
39.37 (6100)	37.31 (0.1325)	H−0(α) → L+1(α); 4d Ru, pic → pic
	37.98 (0.0157)	H−0(β) → L+1(β); 4d Ru, pic → pic
	40.65 (0.0273)	H−4(α) → L+2(α); 4d Ru→4d Ru
		H−3(α) → L+1(α), pic, 4d Ru → pic
	$[Ru(NH_3)_5(4\text{-pic})]^{3+}$ #	
30.00 (~465)	24.85 (0.0133)	H−3(β) → L+0(β), pic, 4d Ru → 4d Ru
	28.31 (0.0018)	H−4(β) → L+0(β), $NH_3 \rightarrow$ 4d Ru
	29.39 (0.0021)	H−6(β) → L+0(β), $NH_3 \rightarrow$ 4d Ru
39.76 (5000)	35.52 (0.0038)	very mixed
	37.78 (0.0073)	very mixed
	38.28 (0.11)	H−0(β) → L+1(β), 4d Ru, pic → 4d Ru, pic
	41.31 (0.035)	H−0(α) → L+0(α), 4d Ru, pic → pic

*Calculated data from *trans*-$[Ru(NH_3)_4(4\text{-pic})(H_2O)]^{3+}\cdot 5H_2O$ (**opt-5a**). #Calculated data from $[Ru(NH_3)_5(4\text{-pic})]^{3+}\cdot 5H_2O$.

were calculated using the geometries **opt-5a** and $[Ru(NH_3)_5(4\text{-pic})]^{3+}\cdot 5H_2O$. In agreement with the experiment, both complexes exhibit spectra formed by weak bands in the visible region arising from LMCT transitions from the ammine ligands to the LUMO (β-d_{xy}) and high-intensity ones in the UV region that were ascribed essentially as intraligand transitions ($\pi \rightarrow \pi^*$). The contribution of the equatorial ligands in the $NH_3 \rightarrow d_{xy}$ transition seems to originate from the CT provided by the interaction with solvent molecules. Nevertheless, as will be shown in the next sections, the assignment of a pure β-d_{xy}

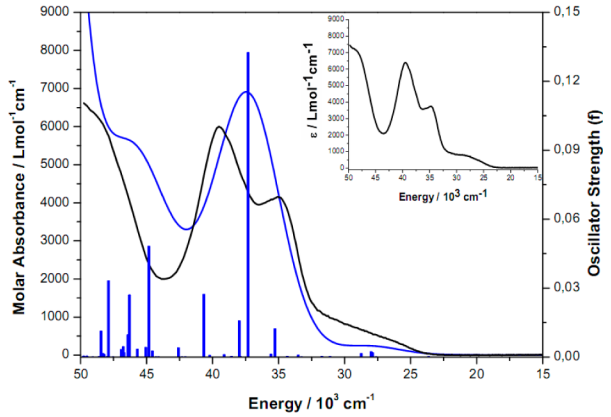

Figure 3. Electronic absorption spectra of *trans*-$[Ru(NH_3)_4(4\text{-pic})(H_2O)]^{3+}$. Blue trace: TD-DFT-calculated spectrum in an IEF-PCM model solvent for the **opt-5a** structure, generated from *GaussSum 3.0* software with half-widths of 5300 cm^{-1} (the electronic transitions are identified by their relative oscillator strengths: blue bars). Black trace: experimental spectrum in aqueous CF_3SO_3H (0.01 mol L^{-1}). Inset: experimental spectrum in acetonitrile.

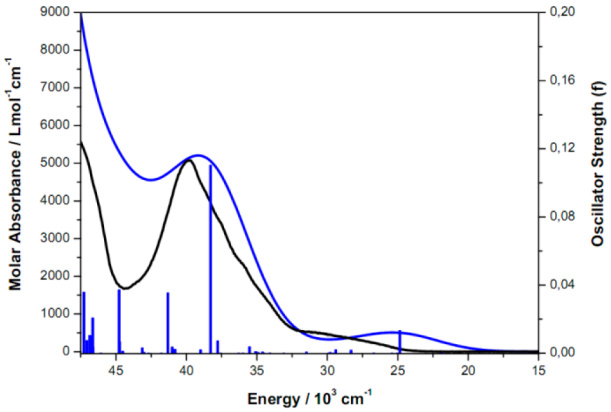

Figure 4. Electronic absorption spectra of $[Ru(NH_3)_5(4\text{-pic})]^{3+}$. Blue trace: TD-DFT-calculated spectrum in an IEF-PCM model solvent with five explicit water molecules, generated from *GaussSum 3.0* software with half-widths of 6500 cm^{-1} (the electronic transitions are identified by their relative oscillator strengths: blue bars). Black trace: experimental spectrum in aqueous CF_3SO_3H (0.01 mol L^{-1}).

function as the LUMO agrees with the nearly axial EPR signal observed in acidic aqueous solution or acetonitrile for *trans*-$[Ru(NH_3)_4(4\text{-pic})(H_2O)]^{3+}$. The LUMO in **opt-5b** and *trans*-$[Ru(NH_3)(4\text{-pic})(OH)]^{2+}$ is a β-d_{xz}-orbital type with 84 and 70% of ruthenium contribution, respectively. The L and 4-picoline contributions in this MO indicate strongly covalent Ru−L bonding. This is reflected in the calculated LMCT transitions HOMO−3 → LUMO (f = 0.0562, 87%) and HOMO−4 → LUMO (f = 0.0488, 33%), where the ground states are bonding orbitals 87 and 63% centered on the 4-picoline ligand, respectively. The HOMO−3 → LUMO transition corresponds to the absorption band calculated in 25 520 cm^{-1} for **opt-5b** shown in Figure 5. Figure 5 also presents the experimental UV−vis spectrum in the solid state of **1**, which presents a CT band in the visible region around 25 000 cm^{-1}. We suggest that the molecules statically positioned in the solid state give an aqua ligand in **1** with features similar to those calculated in **opt-5b**. In this case, interactions between the aqua ligand and solvent molecules are stronger than those in **opt-5a** and promote the aqua ligand

DOI: 10.1021/ic5030857
Inorg. Chem. 2015, 54, 2067−2080

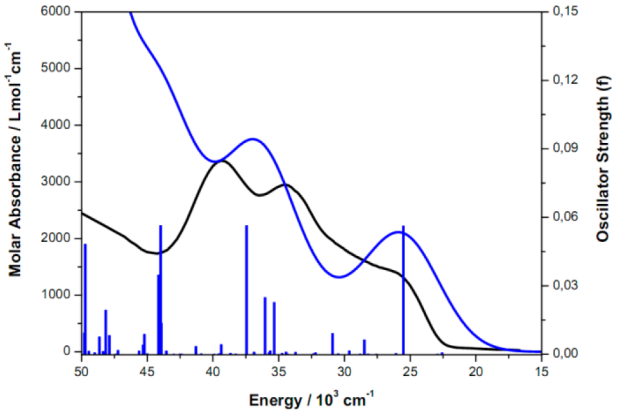

Figure 5. Electronic absorption spectra of *trans*-$[Ru(NH_3)_4(4\text{-pic})(H_2O)]^{3+}\cdot 5H_2O$ (**opt-5b**). Blue trace: TD-DFT (water)-calculated spectrum, generated from *GaussSum 3.0* software with half-widths of 6500 cm^{-1} (the electronic transitions are identified by their relative oscillator strengths: blue bars). Black trace: experimental diffuse reflectance spectrum of **1**. The ordinate in this case is arbitrary and is scaled to match the intensity of the calculated spectrum.

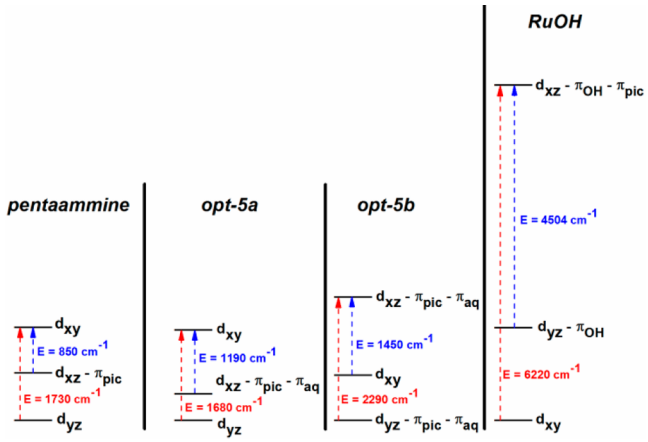

Figure 6. Energy levels of the t_{2g} transitions calculated (TD-DFT) for *trans*-$[Ru(NH_3)_4(4\text{-pic})(L)]^{n+}$, where L = NH_3 (labeled pentaammine), H_2O (labeled **opt-5a** and **opt-5b**), and OH^- (labeled RuOH).

twist with respect to the 4-picoline plane. In agreement with this, the EPR powder spectrum of **1** gave a signal that is *more* rhombic than those in a frozen solution (whether in an aqueous acid solution or acetonitrile; see the EPR Data Analysis section). It would also be desirable to use quantum computational methods to calculate the *g* values for comparison with the experiment. Unfortunately, the Gaussian software has only a rudimentary implementation of the SOC phenomenon and is particularly unsuited to a 4d ion such as Ru^{III}, for which SOC is so dominant (see the LFT discussion) so that fully relativistic quantum-chemical methods are needed.[53,54] Indeed, such computations of spin Hamiltonian parameters of paramagnetic 4d ions are very uncommon. A rare example is the recent work of McNaughton et al.,[55] who studied a Mo^{III} $4d^3$ complex with a LS ($S = {}^1/_2$) ground state.

The first two excited states predicted for **opt-5a**, **opt-5b**, and $[Ru(NH_3)_5(4\text{-pic})]^{3+}\cdot 5H_2O$ in the TD-DFT calculation are attributed to intra t_{2g} transitions with small energy (850−2290 cm^{-1}) and low oscillator strength ($f \leq 0.0002$). The t_{2g} set of orbitals in these transitions are distributed among the *β*-HOMO−1, *β*-HOMO, and *β*-LUMO orbitals, as can been seen in Tables 4 and S6 in the SI. An energy diagram shown in Figure 6 represents the transitions for each geometry. There is a clear destabilization of the MO formed by the $d_{xz} - \pi_{pic}$ antibonding combination in **opt-5b** (LUMO) in comparison with that in **opt-5a** (HOMO). This effect probably originates from the mixing of the d_{xz} and d_{yz} functions on the **opt-5b** MOs, which, in turn, originates from the aqua ligand twist. Overall, a hole in a mixed $d_{xz,yz}$ function gives a reasonably rhombic character to the set of t_{2g} orbitals on **opt-5b** compared to the more axial character of **opt-5a**. However, on the basis of the energy of the excited states, a truly rhombic character is observed only for the pentaammine geometry. In this case, the axial non-*π*-donor ammine ligand and the mixed d_{xz} and d_{xy} functions favor a small ligand-field energy splitting.

EPR Data Analysis. EPR spectra are recognized to be greatly sensitive to energy changes in the t_{2g}^5 orbitals.[56] Assuming an important role for the aqua ligand in both the primary and secondary coordination spheres of Ru^{III}, it is reasonable to evaluate the electronic proprieties of *trans*-$[Ru(NH_3)_4(4\text{-pic})(H_2O)]^{3+}$ as a function of the different solvent environments. Solvent selection was carried out following the experimental Abraham values for the basicity parameter ($\sum\beta^H_2$).[57−59] EPR measurements were performed on complexes **1**−**3**, and the resulting *g* values and ligand-field parameters are summarized in Table 6 (see the EPR Spectra and Solvent Influence section) and will be discussed in the following sections.

LFT Analysis. To gain insight about the energies and electronics features of the d orbitals using EPR experimental data from the above-listed complexes, we begin with a simple octahedral $[Ru(NH_3)_6]^{3+}$ complex with values taken from Harzion and Navon:[60] Racah parameters B = 580(40) cm^{-1}, C = 2300 cm^{-1} ($C/B \approx 4$), Dq = 3480(60) cm^{-1}, which gives the AOM parameter:[61] $\varepsilon\sigma(NH_3) = 10Dq/3 = 11600$ cm^{-1}. Harzion and Navon also reported Dq = 2860(40) cm^{-1} for $[Ru(H_2O)_6]^{3+}$.[60] This value corresponds to $10Dq = 3\varepsilon\sigma + 4\varepsilon\pi$, and we have no way of separating the two bonding contributions; however, we note that Dolder et al.[62] determined $\varepsilon\pi_{\parallel} - \varepsilon\pi_{\perp}$ = 1200 cm^{-1} for $[Ru(H_2O)_6]^{3+}$, so if we assume that one of these contributions is zero, then $\varepsilon\pi(OH_2) \approx 1200$ cm^{-1}, so that $\varepsilon\sigma(OH_2) \approx 8000$ cm^{-1}. Somewhat arbitrarily, we also set $\varepsilon\sigma(N_L)$ = 7000 cm^{-1} for the generic imino donors (i.e., slightly weaker than aqua and much weaker than ammine donors). These crudely estimated bonding parameters will be used for illustrative purposes for the entire series of complexes investigated here by LFT: $[Ru(NH_3)_5(H_2O)]^{3+}$, $[Ru(NH_3)_5L]^{n+}$, *trans*-$[Ru(NH_3)_4L(H_2O)]^{3+}$, and *trans*-$[Ru(NH_3)_4(L)_2]^{n+}$ (used also for *trans*-$[Ru(NH_3)_4(LL')]^{n+}$), where n = 3 for L(′) being a neutral imino ligand, as in most cases, but n = 2 or 1 for complexes with mono- or bisanionic ligands such as $[Ru(NH_3)_5Cl]^{2+}$ or *trans*-$[Ru(NH_3)_4Cl_2]^{+}$.

We then apply an external field of 300 mT, equivalent to X-band resonant fields, i.e., adding spin and orbital Zeeman interactions to yield *g* values. For $[Ru(NH_3)_6]^{3+}$, the isotropic *g* value calculated in this way is extremely sensitive to the choice of k: g_{iso} = 2.204 for k = 1.0, but g_{iso} = 1.898 for k = 0.8, and g_{iso} = 1.974 for k = 0.85, closest to our experimental data [g_{iso} = 1.97 for ($[Ru(NH_3)_6]Cl_3$ in aqueous ethylene glycol (1:1, v/v) (see Figure S8 in the SI)].[63] For generality, we explored the effects of varying k in the range $0.8 \leq k \leq 1.0$ in the other complexes as well. The use of an isotropic k is an oversimplification but necessary to limit the parameter space and provide more general conclusions.

DOI: 10.1021/ic5030857
Inorg. Chem. 2015, 54, 2067−2080

Table 6. Summary of Ligand-Field Parameters for 1−3 as Powder and in Frozen Solution in Different Solvents[a]

complex	solvent	$\|g_1\|$, $\|g_2\|$, $\|g_3\|$	Δ/ζ	V/ζ	V/Δ	k	$\sum\beta^{H}_{2}$
1	aqueous solution	2.735, 2.47, 1.18	1.982	0.506	0.255	0.9017	
	acetonitrile	2.75, 2.435, 1.15	1.944	0.585	0.301	0.8896	0.32
	acetone	2.78, 2.43, 1.10	1.885	0.612	0.325	0.8991	0.49
	propylene carbonate	2.78, 2.43, 1.10	1.885	0.612	0.325	0.8991	
	dimethylformamide	2.83, 2.38, 1.05	1.843	0.753	0.408	0.8993	0.74
	ethylene glycol	2.865, 2.35, 1.05	1.863	0.868	0.466	0.9043	0.78
	2-methoxyethanol	2.885, 2.35, 1.05	1.873	0.901	0.481	0.9149	0.84
	powder	2.925, 2.32, 0.90	1.709	0.888	0.519	0.9017	
2	water/ethylene glycol	2.81, 1.56, 1.20	−0.671	−0.112	0.167	0.9378	
	acetonitrile	2.81, 1.535, 1.215	−0.675	−0.099	0.147	0.9351	0.32
	acetone	2.81, 1.52, 1.26	−0.664	−0.081	0.122	0.9412	0.49
	2-methoxyethanol	2.81, 1.54, 1.26	−0.657	−0.087	0.132	0.9458	0.84
	powder	2.80, 1.60, 1.18	−0.658	−0.131	0.199	0.9398	
3	2-methoxyethanol	2.632, 2.622, 0.50	1.288	0.010	0.008	0.9223	0.84
	powder[b]	2.620, 2.620, 0.60	1.360	0.000	0.000	0.9700	

[a] $\sum\beta^{H}_{2}$: experimental Abraham value, which is used to order the solvents. [b] From ref 20.

We next convert from the hexaammine to $[Ru(NH_3)_5L]^{n+}$, maintaining idealized octahedral geometry: $\theta = 90°$ and $\phi = 0$, 90, 180, and 270° for the equatorial ammines; $\theta = 180°$ and $\phi = 0$ for the axial ammine; θ and $\phi = 0°$ for L(′) (see Chart 1 for the coordinate system). For $[Ru(NH_3)_5L]^{3+}$ with only σ bonding, the complex has idealized C_{4v} point group symmetry, and the above set of Racah and $\varepsilon\sigma$ parameters leads to a ^2E ground state, corresponding to orbital occupancy $d_{xy}{}^2d_{xz,yz}{}^3\{(1/\sqrt{2})[|d^{\pm}_{yz}\rangle \pm |d^{\pm}_{xz}\rangle]\}$ with a very closely lying ($\Delta \approx 50$ cm^{-1}) $^2B_2$ excited state, corresponding to $d_{xy}{}^1d_{xz,yz}{}^4(|d^{\pm}_{xy}\rangle)$. This splitting is the result of a slight mixing of the various $|d^{\pm}_{z^2}\rangle$ and $|d^{\pm}_{x^2-y^2}\rangle$ excited states ($t_2{}^4e^1$ in a strong field representation) into the low-energy states ($t_2{}^5e^0$). This effect is not taken into account in the McGarvey fitting calculation that uses only the states derived from $^2T_{2g}$ ($t_2{}^5e^0$). The next-nearest excited state is a spin quartet, $^4A_2$ ($d_{xy}{}^2d_{xz,yz}{}^2d_{z^2}{}^1$, from $^4T_{1g}$ in O_h, $t_2{}^4e^1$) located at ∼20 000 cm^{-1} above the ground state. A calculation including the SOC and Zeeman effects gives an axial system with $g_\perp = 2.186$ and $g_\parallel = 2.276$. We are not aware of a $[Ru(NH_3)_5L]^{3+}$ complex with which to compare these calculations because L is invariably a π-interacting ligand. Indeed, the key phenomenon in these ruthenium(III) complexes (and many other LS d^5 systems), as has been noted extensively elsewhere, is M−L π bonding.[20,35,62,64−66]

In order to represent in the AOM the structure found crystallographically, L is given the additional twist angle $\psi_L = 45°$, defined from the x axis. This effect (necessarily in combination with noncylindrical, nonzero π bonding) lowers the idealized point group symmetry to C_{2v}. The use of a definition appropriate for σ_d, whereby the d_{xy} orbital has A_1 rather than A_2 symmetry, causes the $d_{xy}{}^1d_{xz,yz}{}^4(|d^{\pm}_{xy}\rangle)$ excited state to be a $^2A_1$ state. The ^2E ground state (in C_{4v}) splits into $^2B_1$ and $^2B_2$ states in C_{2v}, one of which is the ground state and the other is an excited state. These states have different overall d-orbital populations, but in each, the populations of $|d^{\pm}_{yz}\rangle$ and $|d^{\pm}_{xz}\rangle$ are the same (i.e., each is $d_{xy}{}^2d_{xz,yz}{}^3\{(1/\sqrt{2})[|d^{\pm}_{yz}\rangle \pm |d^{\pm}_{xz}\rangle]\}$) so these both can be designated only as $^2B_{(1,2)}$. We employ fully noncylindrical π bonding [$\varepsilon\pi_s(N_L) \neq 0$; $\varepsilon\pi_c(N_L) \equiv 0$]. This choice, when the situation arises (see below) leads to the $|d^{\pm}_{yz}\rangle$ state ($^2B_2$, using the standard definition of C_{2v} symmetry) being the ground state and the $|d^{\pm}_{xz}\rangle$ state ($^2B_1$) being the excited state, which corresponds to $V > 0$, consistent with the McGarvey model (i.e., Δ and V having the same sign).

We again somewhat arbitrarily choose $\varepsilon\pi_s(N_L) = -1000$ cm^{-1}, maintaining $\varepsilon\sigma(NH_3) = 11600$ cm^{-1}, even for the ammine *trans* to L. These simplifying assumptions are necessary to limit the parameter space but, as will be shown below, nevertheless provide valuable illustrations of the electronic structure of these ruthenium(III) complexes.

This π-acceptor interaction of L does not affect the relative energy of the very low-lying ($\Delta \approx 60$ cm^{-1}) $^2A_1$ excited state, but the splitting of ^2E results in a $^2B_{(1,2)}$ excited state lying at ∼1000 cm^{-1} (in the absence of SOC). The symmetry is still axial, but the g values are now in the range seen for $[Ru(NH_3)_5L]^{3+}$ complexes, with significant sensitivity to the choice of k, as seen above for the hexaammine example: $g_\perp = 2.618$, $g_\parallel = 1.473$ ($k = 1.00$); $g_\perp = 2.459$, $g_\parallel = 1.360$ ($k = 0.90$); $g_\perp = 2.379$, $g_\parallel = 1.304$ ($k = 0.85$). That these calculated g values are meaningful can be seen by comparison with entries in Table S11 in the SI. For example, taking $g_\perp = (g_{1(max)} + g_{2(mid)})/2$, $[Ru(NH_3)_5(py)]^{3+}$ has $g_\perp = 2.34$ and $[Ru(NH_3)_5(Him)]^{3+}$ (Him = neutral imidazole) has $g_\perp = 2.50$. The lowest g value ($g_{3(min)} \approx g_\parallel$) in these complexes was not determined but was calculated with the constraints $g_3 < 1.2$ and $k \equiv 0.89$ to be 0.99 and 0.63 respectively for L = py and Him.[64] These g_3 values are lower than our calculated ones, but the difference can be narrowed. On the one hand, acceptable solutions using the McGarvey model could still be found in each case if g_3 were increased by ∼0.1 and, on the other hand, an increase in the magnitude of $\varepsilon\pi_s(N_L)$ leads to lower calculated values for g_3; e.g., $\varepsilon\pi_s(N_L) = -1500$ cm^{-1} yields $g_\perp = 2.501$ and $g_\parallel = 1.076$ ($k = 0.85$).

A final point is the assignment of g values to symmetry axes. The LFT results indicate that $g_{3(min)}$ ($g_\parallel$) corresponds to g_z so that $g_{1,2(max)}$ ($g_\perp$) corresponds to $g_{x,y}$. This is the "expected" result, where the unique axis corresponds to z (here the L−Ru−NH_3 axis). As mentioned above, that orientation (Chart 1) has been found experimentally for $[Ru(NH_3)_5X]^{2+}$, where X^- = Cl^- and Br^-, by single-crystal EPR studies[49] and well extended for similar systems like *trans*-$[Ru(NH_3)_4(Him)(L)]^{3+}$.[64] We need to be clear that the situation for $[Ru(NH_3)_5X]^{2+}$ differs from that for $[Ru(NH_3)_5L]^{3+}$ in that the halido ligand (X^-) is a π donor. Nevertheless, our model is reasonably successful at modeling this system as well. The use of the same parameters for $[Ru(NH_3)_5X]^{2+}$ as those for $[Ru(NH_3)_5L]^{3+}$, except for $\varepsilon\sigma_s(X) = 6000$ cm^{-1} and $\varepsilon\pi_s(X) = \varepsilon\pi_c(X) = 500$ cm^{-1} (i.e.,

DOI: 10.1021/ic5030857
Inorg. Chem. 2015, 54, 2067−2080

weaker σ donation than that for L and cylindrical π donation), yields $g_\perp$ = 1.73 and $g_\parallel$ = 3.03 (k = 1.00), compared to the experiment:[49] $g_\perp$ = 1.25 and $g_\parallel$ = 2.98 (for Cl^-, averaging the observed rhombic g_{min} and g_{mid} values to give $g_\perp$). As is always the case, the parameter space is huge and the system apart from our chief interest in this work, but the chief characteristic, namely, the extreme g value lying along the unique axis, results from our model.

We next consider complexes with two π-interacting ligands, *trans*-$[Ru(NH_3)_4(L)_2]^{n+}$ (n = 3, 2, or 1). Interestingly, *trans*-$[Ru(NH_3)_4(im)_2]^+$ (im = anion of imidazole) exhibits $g_\perp$ = 2.5 and $g_\parallel$ = 1.54,[64] which exactly match the above model for $[Ru(NH_3)_5L]^{3+}$. This implies that the π acidity of the imidazolate anions is less than that of neutral imines, which is reasonable. This effect can be crudely modeled by using smaller magnitude $\varepsilon\pi_s(N_L)$ for both axial ligands: $\varepsilon\pi_s(N_L)$ = −500 cm^{-1} yields $g_\perp$ = 2.361 and $g_\parallel$ = 1.167, while $\varepsilon\pi_s(N_L)$ = −1000 cm^{-1} yields $g_\perp$ = 2.648 and $g_\parallel$ = 0.148 (k = 0.85 for both). Note that *trans*-$[Ru(NH_3)_4(Him)_2]^{3+}$ has g_1 = 3.04, g_2 = 2.20 ($g_\perp \approx$ 2.6), and $g_{3(min)}$ calculated to be 0.15.[64] Here again, we find that $g_{3(min)}$ ($g_\parallel$) corresponds to g_z.

The parameter space available to reproduce experimental g values (even in the simplifying, and erroneous, assumption of axial symmetry) is impossibly large. Not only would there be changes in $\varepsilon\sigma,\pi(E_L)$ (E = N, O, or halide donor atom) as L varies, as touched on above, there is no reason that even the Racah parameters, SOC constant (ζ), or $\varepsilon\sigma(NH_3)$ bonding parameter(s) would not change slightly on going from $[Ru(NH_3)_6]^{3+}$ to $[Ru(NH_3)_5L]^{n+}$ to *trans*-$[Ru(NH_3)_4(L)_2]^{n+}$ (n = 1, 2, 3) or to *trans*-$[Ru^{III}(NH_3)_4(LL')]^{n+}$, which is the proper description of many of the complexes studied earlier.[64]

A final illustration is in order, namely, to show how easily rhombic symmetry, as is found in most cases, can arise. Obviously, if we allow inequivalence among the equatorial ammine ligands, whether by geometry or bonding parameters, or both, a rhombic **g** tensor can result. A more interesting and perhaps more useful means to achieve rhombicity is by simply changing the twist angle for one of the axial π-bonding ligands so that the two are not parallel. In this case, the axial symmetry is lost and the effect is dramatic even for small twists: a change in $\psi_{L'}$ from 45° to 40° yields g_1 = 2.770, g_2 = 2.519, and g_3 = 0.156 [k = 0.85; $\varepsilon\pi_s(N_{L,L'})$ = −1000 cm^{-1}]. In this case, $g_{3(min)}$ still corresponds to g_z and now $g_{2(mid)}$ corresponds to g_y and $g_{1(max)}$ corresponds to g_x. These are the "expected" assignments but, as will be shown below, cannot always be made so easily.

Turning to the complex of interest here, *trans*-$[Ru(NH_3)_4(4\text{-pic})(H_2O)]^{3+}$, we see that this is characterized by $g_\perp \approx$ 2.8 and $g_\parallel \approx$ 1 as a consensus for the results in all solvents, which is similar to the situation modeled above for $[Ru(NH_3)_5L]^{3+}$, where L is a π-acceptor ligand. However, in contrast to the pentaammine complex, where the ligand trans to L is a σ-only donor, in *trans*-$[Ru(NH_3)_4L(H_2O)]^{3+}$ this ligand is a π donor as well. This changes the situation significantly. As described above, on the basis of data for hexaaquaruthenium(III), we will use the following parameters for the aqua ligand: $\varepsilon\sigma(OH_2)$ = 8000 cm^{-1} and $\varepsilon\pi_s(OH_2)$ = 1200 cm^{-1}. These are likely to have changed as a consequence of replacement by both ammine and L, and may also be affected by the solvent, but are sufficient for our illustrative purposes and will not be varied. We can demonstrate that this choice is reasonable by performing a calculation for $[Ru(NH_3)_5(H_2O)]^{3+}$, replacing the bonding parameters for L with those for H_2O. As given in Table 6 (see the EPR Spectra and Solvent Influence section), this complex exhibits a nearly axial EPR spectrum with calculated g = 2.632, 2.622, and 0.50. The use of k = 0.85, as was the case for $[Ru(NH_3)_6]^{3+}$, gives the best match to the experiment: $g_{z(1)}$ = 2.695, $g_{y(2)}$ = 2.679, and $g_{x(3)}$ = 0.366 (the use of k = 0.90 or 1.00 is also reasonable but gives larger values for $g_{z(1)}$ and $g_{y(2)}$ and smaller for $g_{x(3)}$; k = 0.80 gives $g_{1,2}$ values slightly below those of the experiment). Note that this assignment of the axes is the same as that proposed by LaChance-Galang et al. for *trans*-$[Ru^{III}(NH_3)_4(LL')]^{n+}$.[64] The success for $[Ru(NH_3)_5(H_2O)]^{3+}$ allows us to move forward with *trans*-$[Ru(NH_3)_4(4\text{-pic})(H_2O)]^{3+}$. As suggested above by the strong effect on the g values of varying $\psi_{L'}$ in *trans*-$[Ru(NH_3)_4(LL')]^{n+}$, the key parameter is the aqua ligand twist angle, ψ_{OH_2}. This is indeed that case, as shown graphically in Figure 7 and numerically in Table S12 in the SI, where we

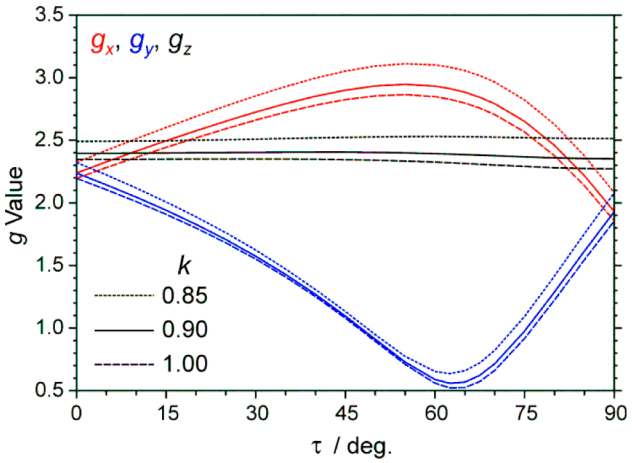

Figure 7. Calculated canonical g values (g_x, red traces; g_y, blue traces; g_z, black traces) for *trans*-$[Ru(NH_3)_4L(H_2O)]^{3+}$ using LFT as a function of the twist angle of the H_2O ligand with respect to L (a planar, imino ligand such as 4-picoline). The twist angle here is defined as $\tau \equiv \psi_L - \psi_{H_2O}$, ψ_L = 45°. The calculation uses (in cm^{-1}) Racah B = 580, C = 2300, and ζ = 800, AOM bonding parameters $\varepsilon\sigma(L)$ = 7000, $\varepsilon\pi_s(L)$ = −1000, $\varepsilon\sigma(OH_2)$ = 8000, $\varepsilon\pi_s(OH_2)$ = 1200, and $\varepsilon\sigma(NH_3)$ = 11600, and ideal octahedral geometry for the location of the donor atoms. Plots generated using three different values of the Stevens orbital reduction factor, k, are shown. Numerical values and further information are given in Table S12 in the SI. Reflection of the pattern about either τ = 0° or τ = ±90° gives the alternate, but equivalent, assignment where g_x is g_{min} and g_y is (generally) g_{max}.

explore the effect on calculated g values of *trans*-$[Ru(NH_3)_4L(H_2O)]^{3+}$ over the entire range, 45° ≤ ψ_{OH_2} ≤ 135°, which is more conveniently given by the difference from alignment of the H_2O ligand with the 4-picoline ligand, $\tau \equiv \psi_L - \psi_{H_2O}$, ψ_L = 45° (see Chart 1). First, a comment is warranted on the electronic structure of *trans*-$[Ru(NH_3)_4L(H_2O)]^{3+}$. When the π bonding of the L and aqua ligands are aligned ψ_{OH_2} = 45°, then the structure is essentially the same as that for $[Ru(NH_3)_5L]^{3+}$, except for the specific energy splittings: the $^2B_{(1,2)}$ ground and excited states are separated by ~2200 cm^{-1}, and the $^2A_1$ excited state lies at ~1300 cm^{-1} above the ground state (absent SOC). However, when ψ_{OH_2} = 0, then the ground state is $^2B_2$ ($|d^{\pm}_{yz}\rangle$), with $^2A_1$ ($|d^{\pm}_{xy}\rangle$) at ~1000 cm^{-1} and $^2B_1$ ($|d^{\pm}_{xz}\rangle$) at ~1500 cm^{-1}. When SOC is included, then the orbital descriptions of the three lowest doublet states are more mixed but are qualitatively the same, with the ground state essentially $^2B_2$ with $^2A_1$ at

DOI: 10.1021/ic5030857
Inorg. Chem. 2015, 54, 2067−2080

~1400 cm^{-1} and $^2B_1$ at ~2200 cm^{-1}. The quartet excited states remain >16 000 cm^{-1} higher in energy.

With this established, we can examine the g values as a function of ψ_{OH_2}. As seen in Figure 7, the value for g_z is nearly constant [~2.4(1), depending on the choice of k], but those for g_x and g_y vary greatly. It is interesting to note that when the π bonding of the L and aqua ligands are nearly aligned, g_z becomes $g_{1(max)}$, the opposite situation from that described above for *trans*-$[Ru(NH_3)_4(LL')]^{n+}$. Moreover, in this situation, all of the g values are above 2.00, which can be modeled using the McGarvey equations only by using $k > 1$. This shows that one should not necessarily reject fits using that type of method (i.e., $^2T_{2g}$-only basis set) when $k > 1$ results. This point has also been made by Sakaki et al.[65,66] The assignment of $g_{3(min)}$ to g_x by LaChance-Galang et al.[64] is appropriate for the range $135° \leq \psi_{OH_2} \leq 215°$ (alternatively, $-45° \leq \psi_{OH_2} \leq 45°$), which is the continuation of Figure 5 either lower to $\tau = -90°$ or higher to $\tau = -90°$. Using Figure 7, a value of $\tau = \pm 75°$ ($\psi_{OH_2} = 120°$, $-30°$) gives g values of 2.7(1), 2.4(1), and 1.0(1), which are roughly those of *trans*-$[Ru(NH_3)_4(4\text{-pic})(H_2O)]^{3+}$ in various solvents, as discussed in the following section.

Another illustration using the data of Table S12 in the SI was performed with the goal to confirm that the orientation of the coordinate system for the g matrix adopted in this work (Chart 1) and based in single-crystal EPR studies of $[Ru(NH_3)_5X]^{2+}$[49] was indeed adequate. Figure 8 shows the calculated g values (at

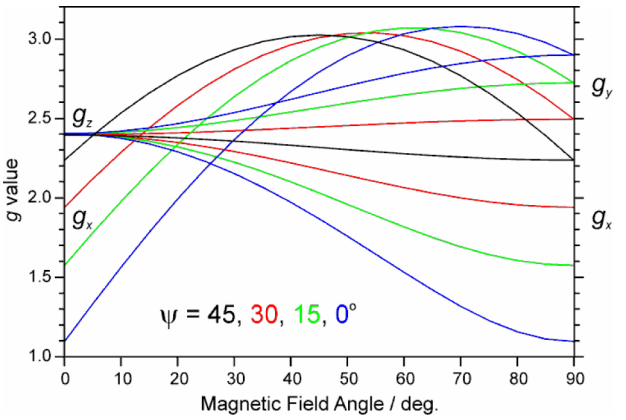

Figure 8. Calculated g values for *trans*-$[Ru(NH_3)_4L(H_2O)]^{3+}$ using LFT as a function of the external magnetic field orientation for ψ_{OH_2} = 45° (black traces), 30° (red traces), 15° (green traces), and 0° (blue traces). For $\psi_{OH_2} = 45°$, there are two (black) curves corresponding to the angle going between g_z and $g_x = g_y$ and between g_x and g_y; for the other angles, there are three (red, blue, and green) curves corresponding to the angle traversing between g_z and g_x, between g_z and g_y, and between g_x and g_y, so that g_x appears on both sides of the graph, while g_z and g_y each appear only once (respectively on the left and right sides of the graph).

300 mT) for the *trans*-$[Ru(NH_3)_4(4\text{-pic})(H_2O)]^{3+}$ complex using the bonding parameters given in Table S12 in the SI, with four different ψ_{OH_2} angles: 45° (lined up with 4-pic), 30°, 15°, and 0° in different orientations of the simulated external magnetic field. We can see that the g_z value remains constant, while the twist of the water ligand with respect to 4-picoline makes the g_x and g_y values diverge greatly. Although the g_z could be the maximum in a few cases or usually the middle g value, the z direction is always N_{pic}–Ru–O_{aq}.

We have shown that, with the use of a LFT model, it is possible to reproduce at least semiquantitatively, the key EPR features of ruthenium(III) complexes with equatorial ammine ligands and a variety of axial ligands, both π donors and π acceptors. We now turn to the experimental EPR data for **1** and related complexes.

EPR Spectra and Solvent Influence. For $[Ru(NH_3)_5(H_2O)](CF_3SO_3)_3$, the following set of EPR parameters have been reported: $g_\perp = (g_1 = g_2) = 2.620$, $0.6 \geq g_\parallel (=g_3) \geq 0$, in powder, water, and propylene carbonate, which yield the following ligand-field parameters: $V = 0$, $0.97 \geq k \geq 0.91$, and $0.99 \leq \Delta/\zeta \leq 1.36$.[20] The set of parameters is typical of axial symmetry ($g_\perp > g_\parallel$; $V/\zeta = 0$) where two of the t_{2g} antibonding $d\pi$ MOs are close and with lesser energy than the third one (so that the "hole" is in the higher, nondegenerate orbital, which is d_{xy}). This result from EPR and LFT is in agreement with that from DFT for **opt-5a**, the result of which predicts a hole in a d_{xy} function higher in energy than two other nearly degenerate 4dπ Ru functions (see Figure 6). The higher energy of the dπ MO was promoted by the π donation of a oxygen electron pair perpendicular to the water molecule plane (**1b$_2$**). In the present work, the $[Ru(NH_3)_5(H_2O)]^{3+}$ EPR spectrum was obtained in a solvent with higher basicity (2-methoxyethanol, $\sum\beta^H_2$ = 0.84). Nevertheless, just a slight difference in the values was observed, $g_1 = 2.632$, $g_2 = 2.622$, and $g_3 = 0.5$, which yielded $V/\xi = 0.01$ and $\Delta/\xi \leq 1.288$ (Table 6). Figure 9 shows the EPR spectra for **1** and **2**, both as powders.

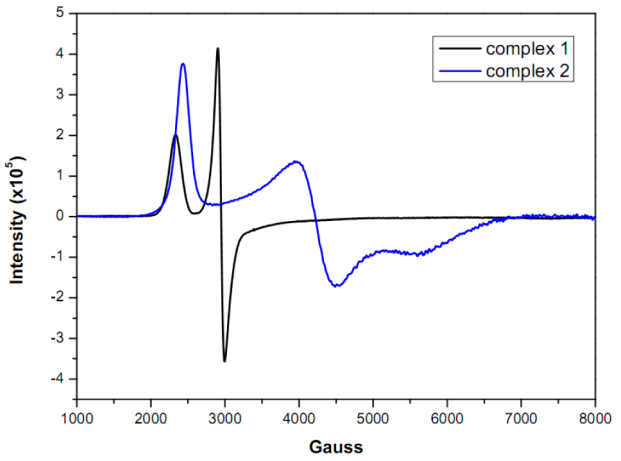

Figure 9. EPR spectra for powder **1** (black trace) and **2** (blue trace) at 77 K.

The EPR spectrum of **1** is composed by two well-defined g values higher than 2.0 ($g_1 = 2.92$ and $g_2 = 2.32$) and a third much smaller than 2.0 ($g_3 \approx 0.9$), while **2** exhibits only one g value higher than 2.0 ($g_1 = 2.80$) and two g values smaller than 2.0 ($g_2 = 1.60$ and $g_3 = 1.18$). In comparison to the complex $[Ru(NH_3)_5(H_2O)](CF_3SO_3)_3$ (axial symmetry, $\Delta/\zeta > 0$ and $V/\zeta = 0$), these set of signals suggest two quite different t_{2g}^5 electronic configuration for both **1** (axial symmetry, $\Delta/\zeta > 0$ and $V/\zeta \neq 0$) and for **2** (rhombic symmetry, $\Delta/\zeta < 0$ and $V/\zeta \neq 0$), see Table 6. For **1**, these signals correspond to a set of t_{2g} orbitals in axial symmetry that has had the degeneracy removed and its rhombic character increased. However, the consequence of the **g** matrix for **2** is that the resulting ligand-field parameters give a negative Δ/ζ value, meaning that the orbital ordering is reversed from the case of **1** and the "hole" is distributed within the two nearly degenerate orbitals. That condition is quite close

DOI: 10.1021/ic5030857
Inorg. Chem. 2015, 54, 2067–2080

to that observed in the DFT calculation, which suggests a rhombic distribution of the t_{2g} orbitals in $[Ru(NH_3)_5(4\text{-pic})]^{3+}\cdot 5H_2O$ (optimized with five explicit water molecules) and a mixed function of d_{xy} and d_{xz}. The π interaction features in the $[Ru(NH_3)_5(4\text{-pic})]^{3+}$ ion cannot be reproduced using the LFT model that yielded Figure 7, which was appropriate for *trans*-$[Ru(NH_3)_4(4\text{-pic})(H_2O)]^{3+}$, so that the orientation of the coordinate system for the **g** matrix of **2** cannot be suggested with confidence. A similar hindrance was reported for $[Ru(NH_3)_5(py)]^{3+}$, which has *g* values and ligand-field parameters[64] quite close to those of **2** (see Table S11 in the SI). For $[Ru(NH_3)_5(4\text{-pic})]^{3+}$, the absence of a π-donor ligand trans-positioned to the 4-picoline ligand seems to decrease the mixing of the 4dπ (Ru) and π^* (4-picoline) orbitals. This was demonstrated by DFT, which suggested the LUMO+1 to be composed of the weak antibonding combination $\pi_{pic(1v)}^*-d_{xz}$ (see Table 4), where the metal contribution is 2%. In this case, the splitting within the 4dπ orbitals has a magnitude similar to that of SOC and thus promotes a highly mixed ground state, as the TD-DFT calculation has suggested (see Figure 6). The DFT calculation suggested the same orbital composition ($\pi_{pic(1v)}^*-d_{xz}$) for *trans*-$[Ru(NH_3)_4(4\text{-pic})(H_2O)]^{3+}$ in the geometry **opt-5a** (aligned 4-picoline and H_2O; see Table 4). In that configuration, the aqua ligand seems to be a poorer π donor than those in **opt-5b** (twisted 4-picoline and H_2O), which can explain why its orbital composition is relatively close to that calculated by DFT for $[Ru(NH_3)_5(4\text{-pic})]^{3+}\cdot 5H_2O$. Interestingly, LFT calculations also suggested that when the π-bonding L and aqua ligands are aligned ($\psi_{OH_2} = 45°$), the structures *trans*-$[Ru(NH_3)_4(L)(H_2O)]^{3+}$ and $[Ru(NH_3)_5(L)]^{3+}$ are qualitatively the same, differing only in the specific energy splitting, which result from the simplified choice of bonding parameters (see the LFT Analysis section).

Our comparison between *trans*-$[Ru(NH_3)_4(4\text{-pic})(H_2O)]^{3+}$ and $[Ru(NH_3)_5(4\text{-pic})]^{3+}$ has demonstrated the aqua ligand π-donor versatility on the $\{[Ru(NH_3)_4(4\text{-pic})]\}$ fragment based on its orientation and interaction with solvent molecules. The *g* values and ligand-field parameters of the powder **1** coherently reflect a structure containing a strong interaction between H_2O and 4-picoline. Experimentally, the contrary condition (aligned ligands) was crudely modeled by tuning the magnitude of the solvent interaction with the aqua ligand using solvents with a range of basicity as parametrized by the Abraham system.[57−59] EPR measurements performed in a wide range of solvents showed a progressive signal differentiation—an increasing rhombicity—as seen in Figure 10. These spectral changes can be correlated with an increase in the solvent basicity ($\sum\beta^H{}_2$; Table 6).

The spectrum in aqueous solution has a signal that is nearly axial, while that in 2-methoxyethanol has significant rhombicity. The rhombicity increase has been associated with the twist angle for one of the axial π-bonding L(′) ligands in *trans*-$[Ru(NH_3)_4(LL')]^{n+}$ by a LFT model, as discussed above. Considering the aqua ligand acidity and the donor character of the solvent, the increased rhombicity in the experimental spectra may be a direct effect of the solvent under the aqua ligand orientation.

Additionally, compared to *trans*-$[Ru(NH_3)_4(4\text{-pic})(H_2O)]^{3+}$, the *g* values and thus the ligand-field parameters in $[Ru(NH_3)_5(4\text{-pic})]^{3+}$ did not change significantly as a function of the solvent. Obviously, the σ-only donor character of the *trans*-NH_3 ligand cannot induce any further effect on the 4dπ Ru

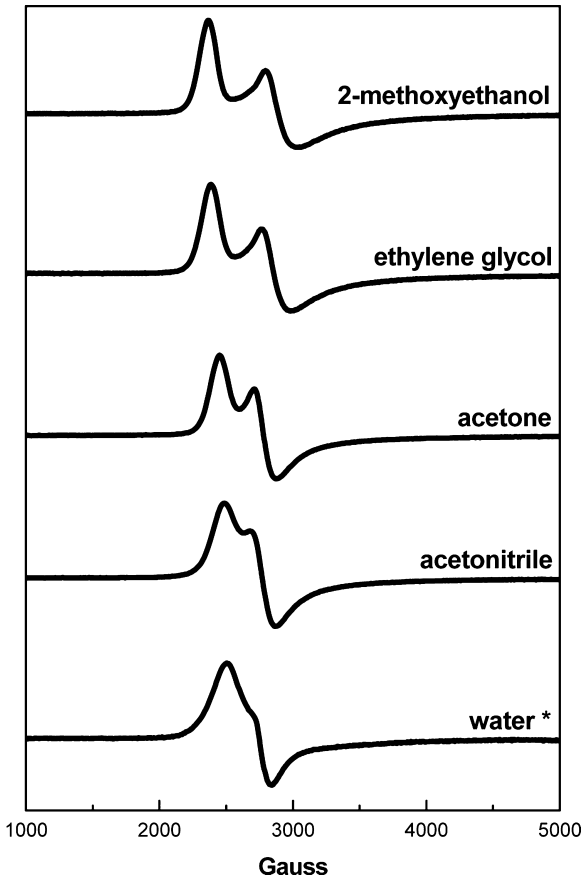

Figure 10. EPR X-band spectra for *trans*-$[Ru(NH_3)_4(4\text{-pic})(H_2O)]^{3+}$ in different frozen solvents, as indicated on the figure: (*) water = CF_3CO_2H solution (1 mM). Experimental conditions: $C_{Ru} = 4 \times 10^{-2}$ mol L^{-1}; temperature = 77 K; frequency range = 9.522184−9.525919 GHz. The spectra are ordered from top to bottom by decreasing the solvent basicity (Abraham values $\sum\beta^H{}_2$[57−59]), which correlates with decreasing EPR spectrum rhombicity.

splitting energies, in contrast to the behavior observed for the aqua ligand with its varying π interaction.

SUMMARY

Coordinated water is an important ligand in controlling the reactivity of ruthenium(III) ammine complexes. Our data on such a representative complex, *trans*-$[Ru(NH_3)_4(4\text{-pic})(H_2O)]^{3+}$, attributes to its aqua ligand an important role on the Ru^{III} t_{2g} orbital energies. The combination of experimental data and theoretical approaches provides a description of the aqua ligand interaction with Ru^{III} as being modulated by the secondary coordinate sphere generated by solvent molecules. DFT calculations have suggested a higher electron density on the aqua ligand oxygen atom when a secondary coordination sphere is provided, exemplified by the calculated geometry **opt-5b**, which exhibits an idealized disposition of water solvent molecules. That effect promotes, in turn, an increased π donation from the aqua ligand to 4dπ Ru orbitals, as well as a greater contribution of the ruthenium into a virtual 4-picoline orbital ($\pi_{pic(1v)}^*-d_{xz}$). However, a comparison of the optimized geometries **opt-5a** (aligned 4-picoline and aqua ligands) and **opt-5b** (unaligned 4-picoline and aqua ligands) suggests that the increased π interaction is heavily dependent on the aqua ligand twist. This effect has likely contributed to the crystallographically observed short bond distances in the

DOI: 10.1021/ic5030857
Inorg. Chem. 2015, 54, 2067−2080

N_{pic}−Ru−O_{aq} axis of **1**. This complex also undergoes a slight decrease in the Ru−OH_2 and Ru−$N_{4\text{-pic}}$ bond distances when cooled from room temperature to 100 K. That process is associated with an increase in the unit cell volume, which is totally reversible upon warming. Such reversibility can be associated with a low-energy phenomenon, such as a hydrogen-bond formation or the aqua ligand twist.

Our studies also shed light on the 4-picoline ligand, relative to ammine or other such ligands. Although 4-picoline exhibits primarily both a σ- and π-donor character in *trans*-$[Ru(NH_3)_4(4\text{-pic})(L)]^{n+}$, its π-acceptor ability is favored by the π^* orbital ($\pi_{pic(1v)}^*$) that lies between the Ru t_{2g} and e_g levels. The unoccupied orbital $\pi_{pic(1v)}^*$ has accepted from the Ru^{III} a portion of the π-electron density donated for L. That effect can offer a mechanism whereby species such as *trans*-$[Ru(NH_3)_4(4\text{-pic})(OH)]^{2+}$, *trans*-$[Ru(NH_3)_4(4\text{-pic})(OOH)]^{2+}$, and *trans*-$[Ru(NH_3)_4(4\text{-pic})(O)]^{2+}$, all containing stronger π donors than H_2O, are generated and their respective fragments, $Ru^{III}OH$, $Ru^{III}OOH$, and Ru^{IV}=O, are partially stabilized. These species are potentially important intermediates in water oxidation catalysis, so that an understanding of their generation, interconversion, and stabilization is of great interest.

■ ASSOCIATED CONTENT

Supporting Information

X-ray crystallographic data in CIF format, data for the crystal structures of **1**·H_2O and **2**·H_2O, detailed DFT and LFT data, *xyz* coordinates, and figures and tables showing the molecular structure, energy, MO compositions, electronic transition assignments, cyclic voltammograms, EPR spectra, and DSC of the ruthenium(III) complex(es) and pK_a determination of the aqua ligand. This material is available free of charge via the Internet at http://pubs.acs.org.

■ AUTHOR INFORMATION

Corresponding Author

*E-mail: douglas@iqsc.usp.br.

Author Contributions

The manuscript was written through contributions of all authors. All authors have given approval to the final version of the manuscript.

Notes

The authors declare no competing financial interest.

■ ACKNOWLEDGMENTS

The authors acknowledge FAPESP and CNPq (Grants 2012/23651-4 and 475631/2011-0, respectively) for financial support and CAPES for the scholarship granted. We are also grateful to Prof. Dr. Bruce R. McGarvey and Prof. Dr. Juares L. Ferreira da Silva for reading and commenting on an early version of our manuscript.

■ DEDICATION

Dedicated to the memory of Professor Joaquim Theodoro de S. Campos.

■ REFERENCES

(1) Pearl, G. M.; Zerner, M. C. *J. Am. Chem. Soc.* **1999**, *121*, 399.
(2) Curtis, J. C.; Sullivan, B. P.; Meyer, T. J. *Inorg. Chem.* **1983**, *22*, 224.
(3) Curtis, J. C.; Blackbourn, R. L.; Ennix, K. S.; Hu, S. X.; Roberts, J. A.; Hupp, J. T. *Inorg. Chem.* **1989**, *28*, 3791.
(4) Ennix, K. S.; Mcmahon, P. T.; Delarosa, R.; Curtis, J. C. *Inorg. Chem.* **1987**, *26*, 2660.
(5) Mahmoud, L.; Gorelsky, S. I.; Kaim, W.; Sarkar, B.; Crutchley, R. J. *Inorg. Chim. Acta* **2011**, *374*, 147.
(6) Naklicki, M. L.; Gorelsky, S. I.; Kaim, W.; Sarkar, B.; Crutchley, R. J. *Inorg. Chem.* **2012**, *51*, 1400.
(7) Ford, P.; Rudd, D. F. P.; Gaunder, R.; Taube, H. *J. Am. Chem. Soc.* **1968**, *90*, 1187.
(8) Shook, R. L.; Borovik, A. S. *Inorg. Chem.* **2010**, *49*, 3646.
(9) Lacy, D. C.; Park, Y. J.; Ziller, J. W.; Yano, J.; Borovik, A. S. *J. Am. Chem. Soc.* **2012**, *134*, 17526.
(10) Escudero, R.; Gomez-Gallego, M.; Romano, S.; Fernandez, I.; Gutierrez-Alonso, A.; Sierra, M. A.; Lopez-Rayo, S.; Nadal, P.; Lucena, J. J. *Org. Biomol. Chem.* **2012**, *10*, 2272.
(11) Sickerman, N. S.; Peterson, S. M.; Ziller, J. W.; Borovik, A. S. *Chem. Commun.* **2014**, *50*, 2515.
(12) Schenk, G.; Neidig, M. L.; Zhou, J.; Holman, T. R.; Solomon, E. I. *Biochemistry* **2003**, *42*, 7294.
(13) Schurmann, K.; Anton, M.; Ivanov, I.; Richter, C.; Kuhn, H.; Walther, M. *J. Biol. Chem.* **2011**, *286*, 23920.
(14) Badiei, Y. M.; Polyansky, D. E.; Muckerman, J. T.; Szalda, D. J.; Haberdar, R.; Zong, R. F.; Thummel, R. P.; Fujita, E. *Inorg. Chem.* **2013**, *52*, 8845.
(15) Bhagan, S.; Sarkar, S.; Wayland, B. B. *Inorg. Chem.* **2010**, *49*, 6734.
(16) Bergquist, C.; Storrie, H.; Koutcher, L.; Bridgewater, B. M.; Friesner, R. A.; Parkin, G. *J. Am. Chem. Soc.* **2000**, *122*, 12651.
(17) Staehle, R.; Tong, L. P.; Wang, L.; Duan, L. L.; Fischer, A.; Ahlquist, M. S. G.; Sun, L. C.; Rau, S. *Inorg. Chem.* **2014**, *53*, 1307.
(18) Barnett, S. M.; Goldberg, K. I.; Mayer, J. M. *Nat. Chem.* **2012**, *4*, 498.
(19) Tfouni, E.; Doro, F. G.; Figueiredo, L. E.; Pereira, J. C. M.; Metzker, G.; Franco, D. W. *Curr. Med. Chem.* **2010**, *17*, 3643.
(20) McGarvey, B. R.; Batista, N. C.; Bezerra, C. W. B.; Schultz, M. S.; Franco, D. W. *Inorg. Chem.* **1998**, *37*, 2865.
(21) Bezerra, C. W. B.; da Silva, S. C.; Gambardella, M. T. P.; Santos, R. H. A.; Plicas, L. M. A.; Tfouni, E.; Franco, D. W. *Inorg. Chem.* **1999**, *38*, 5660.
(22) Shepherd, R. E.; Taube, H. *Inorg. Chem.* **1973**, *12*, 1392.
(23) Brown, G. M.; Sutton, J. E.; Taube, H. *J. Am. Chem. Soc.* **1978**, *100*, 2767.
(24) Ribamar, J. O.; Silva, W. C.; Pereira, J. C. M.; Franco, D. W. *Inorg. Chim. Acta* **2006**, *359*, 2888.
(25) Broomhea, J.; Kanemagu, L. *Inorg. Chem.* **1971**, *10*, 85.
(26) Perrin, D. D.; Almarego, W. L. F. *Purification of laboratory chemicals*; Pergamon Press: Oxford, U.K., 1988.
(27) O'Keefe, T. J.; Yu, P. *Encyclopedia of Materials: Science and Technology*; Elsevier: New York, 2001.
(28) Albert, A.; Serjeant, P. E. *The determination of ionization constant: A laboratory manual*; Chapman and Hall: London, 1971.
(29) Allen, A. D.; Bottomley, F.; Harris, R. O.; Reinsalu, V. P.; Senoff, C. V. *Inorg. Synth.* **1972**, *12*, 2−8.
(30) Vogt, L. H.; Katz, J. L.; Wiberley, S. E. *Inorg. Chem.* **1965**, *4*, 1157.
(31) Isied, S.; Taube, H. *Inorg. Chem.* **1974**, *13*, 1545.
(32) Gaunder, R. G.; Taube, H. *Inorg. Chem.* **1970**, *9*, 2627.
(33) Frisch, M. J.; Trucks, G. W.; Schlegel, H. B.; Scuseria, G. E.; Robb, M. A.; Cheeseman, J. R.; Montgomery, A., Jr.; Vreven, T.; Kudim, K. N.; Burant, J. C.; Millam, J.; Iyengar, S. S.; Tomasi, J.; Barone, V.; Mennucci, B.; Cossi, M.; Scalmani, G.; Rega, N.; Petersson, G.; Nakatsuji, H.; Hada, M.; Ehara, M.; Toyota, K.; Fukuda, R.; Hasegawa, J.; Ishida, M.; Nakajima, T.; Honda, Y.; Kitao, O.; Nakai, H.; Klene, M.; Li, X.; Knox, J. E.; Hratchian, H. P.; Cross, J. B.; Bakken, V.; Adamo, C.; Jaramillo, J.; Gomperts, R.; Stratmann, R. E.; Yazyev, O.; Austin, A. J.; Cammi, R.; Pomelli, C.; Ochterski, J. W.; Ayala, P. Y.; Morokuma, K.; Voth, G. A.; Salvador, P.; Dannenberg, J. J.; Zakrzewski, V. G.; Dapprich, S.; Daniels, A. D.; Strain, M. C.; Farkas, O.; Malick, D. K.; Rabuck, A. D.; Raghavachari, K.; Foresman, J. B.; Ortiz, J. V.; Cui, Q.; Baboul, A. G.; Clifford, S.; Cioslowski, J.;

DOI: 10.1021/ic5030857
Inorg. Chem. 2015, 54, 2067−2080

Stefanov, B. B.; Liu, G.; Liashenko, A.; Piskorz, P.; Komaromi, I.; Martin, R. L.; Fox, D. J.; Keith, T.; Al-laham, M. A.; Peng, C. Y.; Nanayakkara, A.; Challacombe, M.; Gill, P. M.; Johnson, B.; Chen, W.; Wong, M. W.; Gonzalez, C.; Pople, J. A. *Gaussian 03*, revision C.02; Gaussian, Inc.: Wallingford, CT, 2004.
(34) O'Boyle, N. M.; Tenderholt, A. L.; Langner, K. M. *J. Comput. Chem.* **2008**, *29*, 839.
(35) McGarvey, B. R. *Quim. Nova* **1998**, *21*, 206.
(36) Jiang, Y. B.; Telser, J.; Goldberg, D. P. *Chem. Commun.* **2009**, 6828.
(37) Bendix, J.; Brorson, M.; Schaffer, C. E. *Inorg. Chem.* **1993**, *32*, 2838.
(38) Bendix, J.; Steenberg, P.; Sotofte, I. *Inorg. Chem.* **2003**, *42*, 4510.
(39) Forshaw, A. P.; Smith, J. M.; Ozarowski, A.; Krzystek, J.; Smirnov, D.; Zvyagin, S. A.; Harris, T. D.; Karunadasa, H. I.; Zadrozny, J. M.; Schnegg, A.; Holldack, K.; Jackson, T. A.; Alamiri, A.; Barnes, D. M.; Telser, J. *Inorg. Chem.* **2013**, *52*, 144.
(40) Poswal, H. K.; Tyagi, A. K.; Lausi, A.; Deb, S. K.; Sharma, S. M. *J. Solid State Chem.* **2009**, *182*, 136.
(41) Hu, C. H.; Englert, U. *Angew. Chem., Int. Ed.* **2005**, *44*, 2281.
(42) Zhang, J. P.; Lin, Y. Y.; Zhang, W. X.; Chen, X. M. *J. Am. Chem. Soc.* **2005**, *127*, 14162.
(43) Mukherjee, P. S.; Lopez, N.; Arif, A. M.; Cervantes-Lee, F.; Noveron, J. C. *Chem. Commun.* **2007**, 1433.
(44) Maji, T. K.; Mostafa, G.; Matsuda, R.; Kitagawa, S. *J. Am. Chem. Soc.* **2005**, *127*, 17152.
(45) Wang, B. Y.; Xu, W. J.; Xue, W.; Lin, R. B.; Zi-Yi, D. A.; Zhou, D. D.; Zhang, W. X.; Chen, X. M. *Dalton Trans.* **2014**, *43*, 9008.
(46) Silva, H. A. D.; McGarvey, B. R.; Santos, R. H. D.; Bertotti, M.; Mori, V.; Franco, D. W. *Can. J. Chem.* **2001**, *79*, 679.
(47) Silva, H. A. S.; Carlos, R. M.; Camargo, A. J.; Picchi, C. M. C.; Santos, R. H. D.; McGarvey, B. R.; Franco, D. W. *Inorg. Chim. Acta* **2004**, *357*, 3147.
(48) Silva, W. C.; Castellano, E. E.; Franco, D. W. *Polyhedron* **2004**, *23*, 1063.
(49) Kaplan, D.; Navon, G. *J. Phys. Chem.* **1974**, *78*, 700.
(50) Scarborough, C. C.; Sproules, S.; Weyhermuller, T.; DeBeer, S.; Wieghardt, K. *Inorg. Chem.* **2011**, *50*, 12446.
(51) Scarborough, C. C.; Wieghardt, K. *Inorg. Chem.* **2011**, *50*, 9773.
(52) Steiner, T. *Angew. Chem., Int. Ed.* **2002**, *41*, 48.
(53) Ganyushin, D.; Neese, F. *J. Chem. Phys.* **2013**, *138*, 104113.
(54) Autschbach, J. *Philos. Trans. R. Soc., Ser. A* **2014**, *372*, 20120489.
(55) McNaughton, R. L.; Roemelt, M.; Chin, J. M.; Schrock, R. R.; Neese, F.; Hoffman, B. M. *J. Am. Chem. Soc.* **2010**, *132*, 8645.
(56) McGarvey, B. R. *Coord. Chem. Rev.* **1998**, *170*, 75.
(57) Abraham, M. H. *J. Phys. Org. Chem.* **1993**, *6*, 660.
(58) Abraham, M. H. *Chem. Soc. Rev.* **1993**, *22*, 73.
(59) Abraham, M. H.; Platts, J. A. *J. Org. Chem.* **2001**, *66*, 3484.
(60) Harzion, Z.; Navon, G. *Inorg. Chem.* **1980**, *19*, 2236.
(61) Schaffer, C. E.; Jorgense, C. K. *Mol. Phys.* **1965**, *9*, 401.
(62) Dolder, S.; Spichiger, D.; Tregenna-Piggott, P. L. W. *Inorg. Chem.* **2003**, *42*, 1343.
(63) $[Ru(NH_3)_6]Cl_3$ doped into $[Co(NH_3)_6]Cl_3$ exhibit three separate EPR species with very anisotropic **g** tensors that have g_{avg} = 1.93, 1.92, and 1.88. The crystal packing effects that give rise to this anisotropy are absent in frozen solution, and our EPR studies are of only frozen solutions.
(64) LaChance-Galang, K. J.; Doan, P. E.; Clarke, M. J.; Rao, U.; Yamano, A.; Hoffman, B. M. *J. Am. Chem. Soc.* **1995**, *117*, 3529.
(65) Sakaki, S.; Hagiwara, N.; Yanase, Y.; Ohyoshi, A. *J. Phys. Chem.* **1978**, *82*, 1917.
(66) Sakaki, S.; Yanase, Y.; Hagiwara, N.; Takeshita, T.; Naganuma, H.; Ohyoshi, A.; Ohkubo, K. *J. Phys. Chem.* **1982**, *86*, 1038.

DOI: 10.1021/ic5030857
Inorg. Chem. 2015, 54, 2067−2080